

**BURNED FOREST AREA MAPPING FROM POST-FIRE
SENTINEL-2 IMAGERY USING OBJECT-BASED
MACHINE LEARNING CLASSIFICATION**

**NESNE-TABANLI MAKİNE ÖĞRENİMİ
SINIFLANDIRMASI KULLANARAK YANGIN SONRASI
SENTİNEL-2 GÖRÜNTÜLERİNDEN YANMIŞ ORMAN
ALANI HARİTALAMA**

FİDAN ŞEVVAL BULUT

PROF. DR. MUSTAFA TÜRKER

Supervisor

Submitted to

Graduate School of Science and Engineering of Hacettepe University

as a Partial Fulfillment to the Requirements

for the Award of the Degree of Master of Science

in Geomatics Engineering

2024

ABSTRACT

BURNED FOREST AREA MAPPING FROM POST-FIRE SENTINEL-2 IMAGERY USING OBJECT-BASED MACHINE LEARNING CLASSIFICATION

Fidan Şevval Bulut

Master of Science, Department of Geomatics Engineering

Supervisor: Prof. Dr. Mustafa TÜRKER

Co- Supervisor: Prof. Dr. Ayhan ATEŞOĞLU

June 2024, 78 pages

Forest fires cause serious damage not only to the ecosystem in the forest but also to social and economic life. Rapid detection of burned areas with remote sensing methods is important both to determine the current damage and to evaluate the economic and ecological losses caused by the fire and to create rapid response plans. This study presents an approach to identify and map burned forest areas using an object-based random forest (RF) machine learning (ML) classification method using only post-fire Sentinel-2 imagery on the Google Earth Engine (GEE) platform. In addition to original spectral bands of Sentinel-2 (B2, B3, B4, B8, B11, B12), mid-infrared burn index (MIRBI), normalized burn ratio 2 (NBR2), burn area index (BAI) and normalized difference vegetation index (NDVI) bands were calculated and included as additional

bands in the Sentinel-2 image. Prior to object-based classification, image segmentation was carried out using the Simple Non-Iterative Clustering (SNIC) algorithm. Training samples were selected on the GEE platform and object-based classification with the RF algorithm was applied to four study areas (Marmaris – MR, Kavaklıdere – KV, Manavgat – MG, Çanakkale - CK) in Türkiye where forest fires have occurred in recent years. The results showed high performance with an overall accuracy of 93.5% in MR, 97.7% in CV, 94.8% in MG and 96.5% in CK with the object-based RF classifier. In addition, the spatial and temporal transferability of the object-based RF algorithm was evaluated based on two study areas (MG and CK) and the RF model transferability provided an overall accuracy of 87.5% in MR, 94.8% in CV, 93.6% in MG and 96.8% in CK. The results show that burned forest areas can be successfully detected by object-based classification method using cloud-based GEE platform from Sentinel-2 images with a uni-temporal post-fire imagery approach and the potential of developing a transferable object-based classification model for mapping burned forest areas.

Keywords: Forest fire, Object Based Image Analysis, Segmentation, Sentinel-2, Post-fire Image, Google Earth Engine

ÖZET

NESNE-TABANLI MAKİNE ÖĞRENİMİ SINIFLANDIRMASI KULLANARAK YANGIN SONRASI SENTİNEL-2 GÖRÜNTÜLERİNDEN YANMIŞ ORMAN HARİTALAMA

Fidan Şevval BULUT

Yüksek Lisans, Geomatik Mühendisliği Bölümü

Tez Danışmanı: Prof. Dr. Mustafa TÜRKER

Eş Danışman: Prof. Dr. Ayhan ATEŞOĞLU

Haziran 2024, 78 sayfa

Orman yangınları sadece orman içerisindeki ekosisteme değil aynı zamanda sosyal ve ekonomik yaşama da ciddi zararlar vermektedir. Yanmış alanların uzaktan algılama yöntemleri ile hızlı tespitini yapmak hem mevcut hasarın belirlenmesinde hem de yangının yol açtığı ekonomik ve ekolojik kayıpları değerlendirmek ve hızlı müdahale planları oluşturabilmek için önemlidir. Bu çalışmada, yangın sonrasına ait tek tarihli Sentinel-2 görüntüsü kullanarak nesne tabanlı rastgele orman makine öğrenmesi sınıflandırma yöntemi ile yanmış alanların belirlenmesi ve haritalanması için Google Earth Engine (GEE) platformu üzerinden bir yaklaşım sunulmuştur. Sentinel-2'nin ham bantlarına (B2, B3, B4, B8, B11, B12) ek olarak orta kızılötesi yanma indeksi (Mid-Infrared Burn Index - MIRBI), normalize edilmiş yanma şiddeti (Normalized Burn

Ratio 2 - NBR2), yanmış alan indeksi (Burn Area Index - BAI) ve normalize edilmiş bitki indeksi (Normalized Difference Vegetation Index – NDVI) bantları hesaplanmış ve görüntüye ek bantlar olarak dahil edilmiştir. Nesne tabanlı sınıflandırma öncesi basit yinelemesiz kümeleme (Simple Non-Iterative Clustering - SNIC) algoritması ile görüntü segmentasyonu gerçekleştirilmiştir. Eğitim örnekleri GEE platformu üzerinde seçilmiş ve rastgele orman (RO) algoritması ile nesne tabanlı sınıflandırma Türkiye de son yıllarda orman yangını meydana gelen dört çalışma alanına (Marmaris – MR, Kavaklıdere – KV, Manavgat – MG, Çanakkale - CK) uygulanmıştır. Sonuçlar nesne tabanlı RO sınıflandırıcısı ile MR’de %93.5, KV’de %97.7, MG’de %94.8 ve CK’da %96.5 genel doğruluk ile yüksek performans göstermiştir. Ayrıca nesne tabanlı RO algoritmasının mekânsal ve zamansal aktarılabilirliği iki çalışma alanına (MG ve CK) dayalı olarak değerlendirilmiş ve RO model aktarılabilirliği MR’de %87.5, KV’de %94.8, MG’de %93.6 ve CK’da %96.8 genel doğruluk değeri sağlamıştır. Sonuçlar yangın sonrası tek zamanlı görüntü kullanımı yaklaşımı ile Sentinel-2 görüntülerinden bulut tabanlı GEE platformunu kullanarak nesne tabanlı sınıflandırma yöntemi ile yanan orman alanlarının başarılı bir şekilde tespit edilebileceğini ve yanmış orman alanlarının haritalanmasında aktarılabilir nesne tabanlı sınıflandırma modeli potansiyelini göstermiştir.

Anahtar Kelimeler: Orman Yangını, Nesne Tabanlı Görüntü Analizi, Segmentasyon, Sentinel-2, Yangın Sonrası Tek Görüntü, Google Earth Engine

ACKNOWLEDGEMENTS

First and foremost, I would like to thank my supervisor Prof. Dr. Mustafa Türker and my co-advisor Prof. Dr. Ayhan Ateşođlu for their guidance, expertise and encouragement throughout my research journey. Their guidance played an important role in shaping my research skills. It has been an honour to work with them.

I am grateful to my mother, father, and sister for their support, patience, and understanding during this thesis process, as in every period of my life. Their moral support and encouragement at every moment of my life has been invaluable.

TABLE OF CONTENTS

ABSTRACT	i
ACKNOWLEDGEMENTS	v
TABLE OF CONTENTS	vi
LIST OF FIGURES.....	viii
LIST OF TABLES	x
ABBREVIATIONS.....	xi
1. INTRODUCTION.....	1
1.1. Thesis Aims and Objectives	4
1.2. Literature Review	5
2. STUDY AREA & DATA.....	11
2.1. Study Area.....	11
2.2. Data	22
2.2.1 Sentinel-2 MSI Images.....	22
2.2.2. Ancillary Data	24
3. METHODOLOGY	26
3.1. Software Used	27
3.2. Sentinel-2 Data Preprocessing and Spectral Indices	28
3.3. Image Segmentation	29
3.4. Training Data.....	31
3.5. Object-Based Classification	34
3.6. Model Transferability	36
3.7. Accuracy Assessment.....	38
4. RESULTS and DISCUSSIONS	40
4.1. Segmentation	40
4.2. Burned Area Maps.....	51

4.3. Burned Area Maps Based on Model Transferability	54
4.4. Accuracy Values	59
4.5. Inter-comparison with ancillary data	62
5. CONCLUSIONS.....	65
6. REFERENCES.....	68

LIST OF FIGURES

Figure 2.1. Burned forest areas in Türkiye, 2017-2022	11
Figure 2.2. The study areas	13
Figure 2.3. Sentinel-2 satellite image acquired on August 27, 2021 after the fire in the study area MR. The spectral bands B11, B8, and B4 displayed in red, green and blue color planes discriminate between the burned areas and unburned land cover.	14
Figure 2.4. MR management plan according to LULC.....	15
Figure 2.5. Sentinel-2 satellite image acquired on August 17, 2021 after the fire in the study area KV. The spectral bands B11, B8, and B4 displayed in red, green and blue color planes discriminate between the burned areas and unburned land cover.	16
Figure 2.6. KV management plan according to LULC.....	17
Figure 2.7. Sentinel-2 satellite image acquired on August 09, 2021 after the fire in the study area MG. The spectral bands B11, B8, and B4 displayed in red, green and blue color planes discriminate between the burned areas and unburned land cover.	18
Figure 2.8. MG management plan according to LULC.....	19
Figure 2.9. Sentinel-2 satellite image acquired on August 28, 2023 after the fire in the study area CK. The spectral bands B11, B8, and B4 displayed in red, green and blue color planes discriminate between the burned areas and unburned land cover.....	20
Figure 2.10. CK management plan according to LULC.	21
Figure 3.1. Workflow of the methodology	26
Figure 3.2. MR Study Area Training Data Set	32
Figure 3.3. KV Study Area Training Data Set	33
Figure 3.4. MG Study Area Training Data Set	33
Figure 3.5. CK Study Area Training Data Set	34
Figure 3.6. The RF Algorithm.....	35
Figure 4.1. The result of SNIC segmentation for study area MR	42
Figure 4.2. The segments in vector form for study area MR (Seed size: 50).....	43
Figure 4.3. The result of SNIC segmentation for study area KV.....	44
Figure 4.4. The segments in vector form for study area KV (Seed size: 50).....	45
Figure 4.5. The result of SNIC segmentation for study area MG	46
Figure 4.6. The segments in vector form for study area MG (Seed size: 50).....	47
Figure 4.7. The result of SNIC segmentation for study area CK	48
Figure 4.8. The segments in vector form for study area CK (Seed size: 50).....	49
Figure 4.9. The result of SNIC segmentation for study area MR. a) seed size: 25, b) seed size: 50, c) seed size: 150, d) seed size: 250.....	50

Figure 4.10. Several examples (red circled areas) for illustrating over-segmentation from study area MR (Seed size: 50).	51
Figure 4.11. Burned-area map of study area MR obtained through object-based RF classification of the post-fire Sentinel-2 image.	52
Figure 4.12. Burned-area map of study area KV obtained through object-based RF classification of the post-fire Sentinel-2 image.	52
Figure 4.13. Burned-area map of study area MG obtained through object-based RF classification of the post-fire Sentinel-2 image.	53
Figure 4.14. Burned-area map of study area CK obtained through object-based RF classification of the post-fire Sentinel-2 image.	53
Figure 4.15. Burned-area map of MR obtained through transferability of the RF model.	54
Figure 4.16. Burned-area map of KV obtained through transferability of the RF model.	55
Figure 4.17. Burned-area map of MG obtained through transferability of the RF model.	55
Figure 4.18. Burned-area map of CK obtained through transferability of the RF model.	56
Figure 4.19. (a) For a selected region of MG, false color display of the post-fire Sentinel-2 image. (b) Burned-area map obtained by using RF model. (c) Burned-area map obtained by using RF model transferability. (d) For a selected region of MR, false color display of the post-fire Sentinel-2 image. (e) Burned-area map obtained by using RF model. (f) Burned-area map obtained by using RF model transferability.	58
Figure 4.20. For all study areas, the confusion matrices computed for the RF model and RF model transferability.	60
Figure 4.21. PA and UA values computed for the RF model and RF transferability	61
Figure 4.22. For study area KV, comparison of the detected burned areas (shown in red color) with the burned areas provided by the data sets MCD64A1, C3SBA10, and EFFIS. *GDF data was not included as it is not in spatial form.	64

LIST OF TABLES

Table 2.1. MR management plan according to LULC and tree species on hectare base.....	15
Table 2.2. KV management plan according to LULC and tree species on hectare base.	17
Table 2.3. MG management plan according to LULC and tree species on hectare base.	19
Table 2.4. CK management plan according to LULC and tree species on hectare base.	21
Table 2.5. Sentinel-2 MSI Bands.	22
Table 2.6. The Sentinel-2 images used in this study.	23
Table 2.7. The Sentinel-2 MSI bands used in this study.	23
Table 3.1. Spectral indices used in this study.....	29
Table 3.2. The number of samples used for accuracy validation	38
Table 4.1. OA and Kappa coefficients resulting from object-based RF classification and RF model transferability for all study areas.	60
Table 4.2. Comparison of the burned areas detected in this study with the burned-areas provided by the data sets MCD64A1, C3SBA10, EFFIS, and GDF. *The C3SBA10 dataset did not contain burned area information for study area CK . The values are in hectars.	63

ABBREVIATIONS

Symbols

ha	Hectare
Mha	Million Hectares

Abbreviations

ASTER	Advanced Spaceborne Thermal Emission and Reflection Radiometer
BAI	Burn Area Index
EFFIS	European Forest Fire Information System
EM	Error Matrix
EMS	Emergency Management Service
ESA	European Space Agency
EVI	Enhanced Vegetation Index
FRA	Forest Resources Assessment
GDF	General Directorate of Forestry
GEE	Google Earth Engine
LULC	Land Use & Land Cover
MIRBI	Mid-Infrared Burn Index
MODIS	Moderate Resolution Image Spectroradiometer
MSI	Multispectral Image

NBR	Normalized Burn Ratio
NBR2	Normalized Burn Ratio 2
NDVI	Normalized Difference Vegetation Index
OA	Overall Accuracy
OBIA	Object Based Image Analysis
OLI	Operational Land Imager
PA	Producer's Accuracy
RF	Random Forest
SLIC	Simple Linear Iterative Clustering
SNIC	Simple Non-Iterative Clustering
SVM	Support Vector Machine
UA	User's Accuracy

1. INTRODUCTION

Forests are important for protecting and ensuring the sustainability of the ecosystem structure with a holistic approach, with their ecological, biological and landscape resource values [1]. Forests constitute approximately 1/3 of the world's land. According to the Global Forest Resources Assessment (FRA) 2020 report, the global forest asset in 2020 was 4058931 ha. According to the same report, the European region constitutes 25% of the world's forest areas. This rate is followed by South America at 21%, North and Central America at 19%, Africa at 16%, and Asia at 15%. According to the FRA 2020 report, the global forest acreage fell by over 178 million hectares between 1990 and 2020.

Forests experience many degradations that can affect their health, vitality and ability to provide a wide range of products and ecosystem services. Forest fires, insects, diseases and severe weather events are among these degradations [2]. Although forest fires are part of the cycle within the ecosystem as a whole due to regeneration, nutrient cycling, habitat diversity and control of pests and diseases, they are one of the increasing anthropogenic and disturbing events that affect ecosystems, biodiversity and human health [3, 4].

Forest fires caused about 29% of global tree cover loss between 2001 and 2023. From 2001 to 2023, a total of 154 million hectares (Mha) of tree cover was lost worldwide due to wildfires [5]. When the forest cover is evaluated for Türkiye, according to the FRA 2020 report, Türkiye ranked 27th in the world in terms of forest area in 2020 [2]. According to the statistics of the General Directorate of Forestry (GDF), the total forest assets in 2022 is 23245000 ha, of which 22248680 ha are high forest and 996320 ha are coppie forest [6]. When losses due to forest fire are evaluated for Türkiye, according to GDF data, 76931 fires occurred between 1998-2022. In the last 5 years, the worst fire seasons have been seen for the country, and an area of 202242 ha forest was burned between 2017 and 2022 [6]. Figure 2.1 shows the number of fires and the amount of burned area annually between 2017 and 2022. When the data between 2013 and 2022 was analyzed, it was observed that forest fires larger than 500 ha occurred between June and September, especially in July and August.

In recent years, the frequent and widespread occurrence of forest fires on a global scale has put the issue of forest fire prevention and mitigation on the agenda. Within the framework of sustainable forest management for the continuity of the ecosystem, determination of fire risk, determination of burned and destroyed areas, determination of fire severity, determination of the extent of damage are important for future planning [7-12]. Therefore, information on the extent of forests burned in countries in the past, mostly from terrestrial surveys, has been used to generate data on a global scale. However, the accuracy of statistical data reported by countries is often criticized as being based on outdated, incomplete or opaque methods. At the same time, although country data are obtained through field studies, there are concerns about data precision and accuracy. The inaccessibility of data for some countries is also a problem. Therefore, the differences in methodologies adopted by countries and the inadequacy of institutions in collecting and storing data have made these sources unreliable when making global or regional analyses [13]. For this reason, with the beginning of satellite observations, satellite images have begun to be used as a reliable alternative for burned area detection [14]. Satellite images are used for early detection of forest fires [15], monitoring their behavior [16], assessing damage [17], identifying hot spots [18], monitoring air quality [19], mapping [20], monitoring and modeling fire severity [21].

Satellite imagery provides significant convenience in terms of time and labor for the detection and mapping of burned areas. Although high-resolution data can be obtained with commercial satellites, the high cost is the biggest obstacle to its use [22]. Free access to medium resolution and low temporal resolution satellite images offers significant advantages in mapping burned forest areas [23]. Particularly open source and free satellite images with medium geometric resolution, such as Landsat and ASTER/Terra, MODIS/Terra are preferred for national and global scale studies [22, 24, 25]. For all that, in the recent past, OLI/Landsat-8, MSI/Sentinel-2 satellite images with better spatial resolutions have begun to be used more frequently to obtain more sensitive and accurate results [12, 26-28].

Majority of current applications for identifying and mapping burned forest areas are based on a bi-temporal approach that allows the identification of burned areas as a result

of changes in between the pre-fire and post-fire images due to reduced vegetation cover [12, 29-31]. In contrast, the uni-temporal approach only focuses on analyzing post-fire images and is faster to implement. Unlike the bi-temporal approach, it does not have disadvantages due to differences in phenology, sensor calibration or atmospheric effects. It eliminates the disadvantage of finding images with low cloud cover for two different times. However, the uni-temporal approach may have difficulties for areas that may be confused with the burned area due to the lack of reference images before the fire [29].

Images collected by different sensors and different methods have been used for the detection and mapping of burned areas. Pixel-based and object-based image analysis have been the two main approaches used in the classification of satellite images [32]. In previous years, several studies have employed object-based logic for the classification of satellite images with different resolutions in mapping burned areas as object-based approaches provide more accurate results than the pixel-based approaches [8, 33-35]. [36] has demonstrated that object-based image classification provides promising results in the field of burn area mapping.

Although object-based image analysis techniques have proven to be effective in image classification, studies utilizing object-based classification with Sentinel-2 images for the detection of burned areas in the context of forest fires are limited [37]. In the study conducted by [38], 173 scientific papers were reviewed on supervised object-based land-cover image classification and it was concluded that the Random Forest (RF) algorithm is the best performing algorithm for object based classification and the most widely used algorithm in recent years. The RF algorithm is followed by the support vector machine (SVM) algorithm. These two algorithms are considered to be the most efficient and frequently used algorithms for satellite image classification [39].

Evaluating the transferability of machine learning (ML) algorithms is a crucial step for generalization, showing how the model can be trained in one place or at a time and how it can be used in different domains and times, and the generalization of classification results [40]. In recent years, the spatial transferability of ML models has been

successfully applied in land cover classification and crop type classification [41]. Likewise, the spatial and temporal transferability methods were successfully applied for the detection of burned forest areas and burn severity from the satellite images with different resolutions [36, 37, 39, 42, 43].

In the last few years, with the increasing availability of remote sensing data, cloud-based platforms have been developed rapidly, enabling individuals to access and analyze geospatial data using web-based interfaces [44]. Google Earth Engine (GEE) is a cloud-based platform that leverages Google's enormous computing capabilities to a range of high-impact societal issues, including planetary-scale geospatial analysis [45]. By leveraging the vast archive of satellite imagery and the computational capabilities of GEE, researchers, land managers, and policymakers can effectively monitor and manage forest fires at regional and global scales.

1.1.Thesis Aims and Objectives

In this research study the main aim is to map burned forest areas using an object-based RF ML classification method from only the post-fire Sentinel-2 imagery, which is one of the open-source earth observation data on the cloud-based GEE platform. The other aim of the study is to evaluate the spatial and temporal transferability of the object-based RF algorithm in detecting burned forest areas on the GEE platform and achieve high classification accuracy in different test areas.

The goals of the thesis are as follows:

- To evaluate the performance of the object-based RF algorithm for detecting burned forest areas using the uni-temporal Sentinel-2 data on the GEE platform.
- To evaluate the spatial and temporal transferability of the object-based RF algorithm in detecting burned forest areas in different study sites on the GEE platform.
- To determine appropriate parameter values for the simple non-iterative clustering (SNIC) segmentation algorithm, which will be used for the segmentation of the image into image objects.

- To evaluate the success of object-based image classification and spatial transferability in detecting the burned forest areas in different study sites with different land cover types.
- To quickly estimate fire damages and increase the effectiveness of rapid disaster management for potential future fires in Mediterranean forests in Türkiye with Sentinel-2 data using the open-source GEE platform.

1.2.Literature Review

Historically, organizations have obtained burned area information from fire management teams. The different methods used by countries and the inadequacies of institutions in data collection and storage have made these sources unreliable when conducting global or regional analyses. With the introduction of satellite observations, satellite images have started to be used as a robust alternative for burned area detection [14]. Satellite imagery significantly facilitates the identification and mapping of burned areas in terms of time and labor. Rapid and accurate mapping of burned areas contributes to post-fire damage assessment, planning studies, vegetation restoration studies and reforestation studies [46].

The use of satellite imagery within the framework of forest fires is widely used in many kinds of research, including pre-fire predictions, hazard, risk, susceptibility analyses, fire severity, burning area detection, monitoring and evaluation of burning areas [47-50]. Although the use of satellite imagery for the detection and mapping of burned areas has a long history, there are still active studies and research integrating object oriented and ML methods [14]. In addition, studies on the detection of forest fires and mapping burned areas from Sentinel-2 images using object-based classification approaches are still limited [37]. In this part of the thesis, mostly object-based and ML integrated studies and studies using Sentinel-2 for the detection of burned forest areas are included.

In the study conducted by [33], a methodology was applied to map burned areas with Sentinel-2 satellite images, aiming to minimize user interaction. The Mean-Shift

segmentation technique was used to generate image objects for the object-based image analysis. The fuzzy C-means clustering technique automatically selects a small section of the typical images object as the training set. The authors applied burned area indices on pre-fire and post-fire images to label training models. They used the pre-post fire index differences (MIRBI, NBR2, NDII, NDWI) to label the training model with a set of empirical threshold values. The methodology produces high accuracy burned area maps and requires minimal user interaction [33].

In the study conducted by [34] on Kangaroo Island, South Australia, burned areas and land uses were classified using multi-resolution segmentation and hierarchical classification. The burned areas, which were seriously affected by the 2019-2020 forest fire, were mapped and the severity of the fire was evaluated from Landsat 8 images using the GEE platform. The authors describes the importance of using a multi-source data approach to more accurately define burned areas and their approach provides an overall accuracy of 90.2% [34].

In the study conducted by [51], the results of object-based and pixel-based classification approaches were compared. A new set of rules to be used in a decision tree-based classification was created and SPOT-6 images were used. It was suggested that relying solely on normalized vegetation index thresholds for object-based classification is insufficient for mapping burn areas. The authors emphasized that the post-fire image may be the only source due to the difficulties in obtaining pre-fire images in some cases and compared their studies with single source and two sources separately. The results demonstrate that, in both cases, misclassification tended to rise as a result of shadows. There were other aspects that made the ML categorization challenging, such as different forms of the forest canopy and the mixing of the plants. It was shown that object-based classification can deduce boundaries of forest types. The burned region was mapped with the kappa value of 0.9322 in object-oriented classification, whereas the kappa value of 0.7433 was computed from the pixel-based classification [51].

In the study conducted by [8], the performance of RF algorithm was tested in extracting burned forest areas with multi-resolution segmentation technique. To detect burned

areas, variables such as brightness, maximum difference, average values of six bands and spectral indices were selected and RF model was used for the classification. The study areas used include Kumluca and Adrasan regions, which are two forest areas burned on the same date. An accuracy of 0.99 was achieved and the usability of the method for detecting burned areas was demonstrated [8].

In the study conducted by [52], a combination of rule-based and supervised classification methods was employed alongside image segmentation to detect burned areas. A primary objective of the research was to delineate burned and unburned areas through the integration of spectral indices. The accuracy of the results was determined by comparing them with those of the Copernicus Emergency Management Service (EMS) maps. The findings revealed that the rule-based approach demonstrated an agreement of 86.9% for Landsat 8 imagery and 85.4% for Sentinel 2 imagery. On the other hand, the supervised classification method exhibited higher agreement rates, with 88.6% for Landsat 8 imagery and 90.7% for Sentinel 2 imagery. The performance of the RF algorithm was evaluated in mapping burned forest areas using the multi-resolution segmentation technique. To detect burned areas, variables such as brightness, maximum difference, average values of six bands and spectral indices were selected and RF model was used for the classification. The study areas used include Kumluca and Adrasan regions, which are two forest areas burned on the same date. An accuracy of 0.99 was achieved and the usability of the method for detecting burned areas was demonstrated [52].

[53] integrated empirical approaches based on different spectral indices and supervised classification to identify and map burned areas. To train and validate the classifier, 64 forest fires that occurred in Greece between 2016 and 2019 were taken as the reference. The Extreme Gradient Boosting (XGB) algorithm was combined with an empirical approach to select training models with difference spectral indices, and an automatic classification workflow was presented for the purpose of operating the approach in a national operating framework. Average overall accuracy of 98% was achieved, as well as high precision, recall, and F1 score values [53].

In the study conducted by [54], an automatic method is presented for detecting burned areas via Sentinel-2 time series imagery. The algorithm includes optimal spectral indices, single-dual-temporal images, and MSI images, integration of multi-source active fire products, an interannual time series, and adaptive threshold post-processing for large burned areas. The algorithm uses GEE and local computation, and is tested on different land cover and large areas such as forests, croplands, shrublands, grasslands, savannas. The results were compared with existing MCD64A1, FireCCI51, LBA_CU, and FireCCISFD20 burned area products. The method automatically mapped burned areas at various land cover and regional scales and improved the membrane coefficient by about 7% and 9% compared to medium resolution burned area products [54].

In the study conducted by [55], active fires identified from Terra and Aqua MODIS sensors and Sentinel-2 MSI reflectance measurements were used to create a locally adapted multi-temporal two-phase burn area algorithm. The whole of Sub-Saharan Africa was analyzed between January and December 2016. The product displayed accuracy values higher than those of current worldwide burn area offerings. After applying the burn area algorithm to more than 11,000 Sentinel-2 images, a database containing minor fires (less than 100 ha) was produced. Demonstrating the practical potential of these tools to improve understanding of the impacts of wildfires worldwide, this is the first continental burn area product produced with medium resolution sensors. Additionally, spectral sensitivity analysis was performed to determine appropriate bands and indices for the detection of sub-Saharan African burned areas. The algorithm employs the NDVI, Enhanced vegetation index (EVI), Normalized Burn Ratio (NBR), and BAI indices in various spaces. The proposed methodology aims to improve mapping accuracy, especially for small fires missed by global burned area products [55].

Using Sentinel-2 satellite imagery, [29] investigated how well the Normalized Burn Ratio Plus (NBR+) index can map the burned areas. It was found that when there are clouds and bodies of water, the NBR+ index performs better than other indices. Utilizing both uni-temporal and bi-temporal methods, the study evaluated the NBR+ index in Sicily in comparison to five other indices. Areas incorrectly identified as

burned by other indices because of clouds or bodies of water were effectively excluded by the NBR+ index. The authors discuss the benefits and drawbacks of post burned image analysis utilizing a uni-temporal vs a bi-temporal method. By concentrating just on post-burn images, the single-date strategy is quicker and eliminates inaccuracies caused by phenological variations, pixel misregistration, sensor calibration, sun-sensor geometry, and atmospheric influences. There would be problems in mapping regions that have recurring spectral signatures, such as water and wilted plants, as these areas might be confused with the burned areas. The bi-temporal technique, on the other hand, offers a more thorough analysis but necessitates careful consideration of cloud cover and image availability at various times [29].

[37] proposed an approach to automatically select training areas and perform object-based classification to evaluate forest fire damage from Sentinel-2 images in GEE environment. For classification, three ML algorithms – RF, SVM, and CART were used. The transferability of the proposed method was also evaluated and it was concluded that RF was the most effective algorithm providing overall accuracies of 97.6% and 93.8%, respectively in study areas Uljin and Gangneung [37].

[39] investigated the potential for burn severity mapping from Sentinel-2 imagery using ML algorithms and transferability of the model. RF and SVM algorithms were used with a pixel-based classification approach. Eight spectral indices were also included in the classification. In addition, the transferability of the model created on forest fires occurring in similar areas was evaluated and fire damage classification was performed. It was conducted based on the tests in the Portuguese forest area that the RF algorithm performed better than the SVM algorithm. Furthermore, the results confirmed that Copernicus EMS data can be transferred as a reference for fire damage classification in potential areas [39].

[42] developed a model for mapping burned areas in Greece using Landsat imagery and object-oriented classification logic. The performance of object-oriented classification in the Mediterranean region was demonstrated. The results were also compared with the results of pixel-based classification. In order to evaluate the transferability of the

developed model, the model was tested in a burned area in Spain. The results showed that the developed object-oriented method was successfully applied with an overall accuracy of 98.85%. The results also showed that the performance of object-oriented classification was higher than pixel-based classification and that the model was successful and transferable when tested in a slightly different study area in Spain [42].

2. STUDY AREA & DATA

2.1. Study Area

Türkiye has a rich ecological diversity with an area of 78 million ha, and according to the findings made as of 2020, 29.4% of this area is covered by forest areas [6]. Forest fires in Türkiye are generally concentrated in the southern and western regions of the country, especially along the Mediterranean and Aegean coasts. These regions are often characterized by high temperatures and low humidity levels during hot, dry summer months, contributing to more frequent and severe wildfires [56].

According to annual reports published by European Forest Fire Information System (EFFIS), approximately 57% of Türkiye's forest area (12.5 million ha) is located in fire-sensitive areas. 2021 was Türkiye's worst fire season in more than a decade. According to the same report, the total burned area resulting from 612 fires was 206,013 ha; This is the highest amount recorded in Europe, the Middle East and North Africa in 2021 [57]. The forest areas affected by the fires in Türkiye that occurred between 2017 and 2022 are shown in Figure 2.1 [6].



Figure 2.1. Burned forest areas in Türkiye, 2017-2022

In this research work, the study areas were selected among the major forest fires occurred in Türkiye in recent years. The selected areas are located in the Muğla - Marmaris region (MR), Muğla - Kavaklıdere region (KV), Antalya - Manavgat region (MG), where a forest fire occurred in 2021, and in the Çanakkale region (CK), where a forest fire occurred in 2023. The distribution of the study areas on the map is shown in Figure 2.2. For the selection of the study areas, care was taken to ensure that the burned areas and study areas represented different land use & land cover (LULC) such as forest, agriculture and settlement. The behavior of fire may differ in different land cover types. Moreover, since fire can occur not only in homogeneous forested areas but also in heterogeneous forested areas, test areas with different land cover distribution were selected. Although the selected study areas have the characteristics of Mediterranean forests, they contain a combination of forest types, a diversity of land use classes and different topographic conditions.

Study Area MR: This study area is located within the borders of Muğla province of Türkiye. An area of 32,328.04 ha, including burned forest areas, was selected to test the proposed methodology and is shown in Figure 2.3. Based on the European Space Agency (ESA) WorldCover 10 m product based on Sentinel-1 and Sentinel-2 imagery, the study area in 2021 includes 19089.5 ha of trees, 2471.7 ha of shrubland, 1286.1 ha of grassland, 252.3 ha of cropland, 840.9 ha of built-up, 122.6 ha of barren/sparse vegetation, 8263 ha of open water, and 1.7 ha of herbaceous wetland. In this area, the dominant tree species is red pine. Of the forest area, 39% is degraded stand, 20% is high forest land and 25% includes Maquis vegetation (Figure 2.4 & Table 2.1). According to the long-term measurements of the General Directorate of Meteorology, the yearly average temperature of Muğla province is 15.1°C, the yearly average maximum temperature is 21.3°C, and the yearly minimum temperature is 9.6°C. The average monthly total rainfall is 1206.1 mm. According to the Koppen-Trewartha climate classification, the region has a subtropical dry summer climate, and Mediterranean climate. The forest fire in the region started on July 29, 2021 and continued for 8 days. Although the majority of the burned area is forest area, cropland and settlements areas are also among the burned areas.

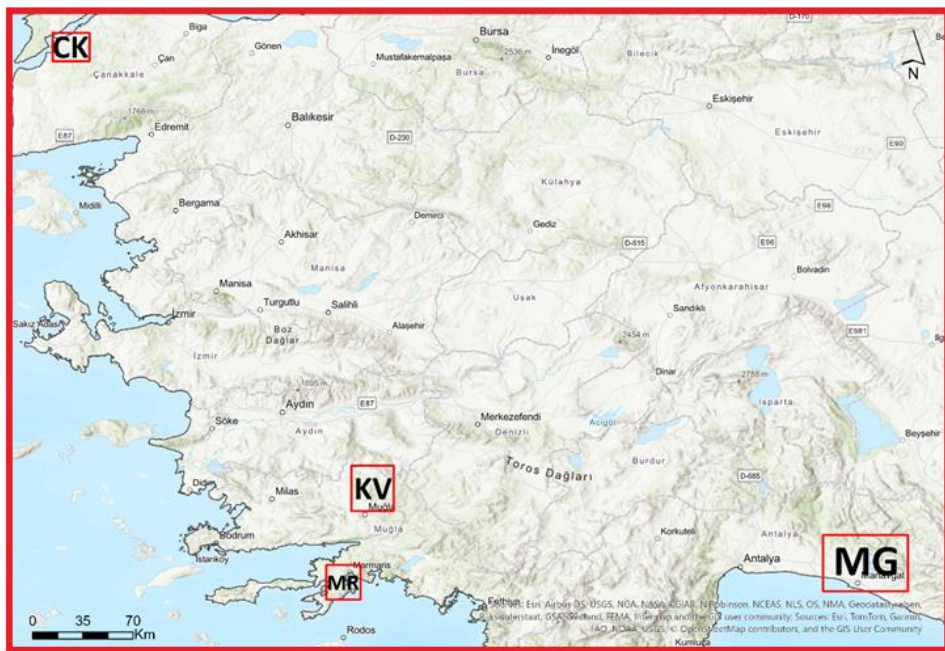


Figure 2.2. The study areas

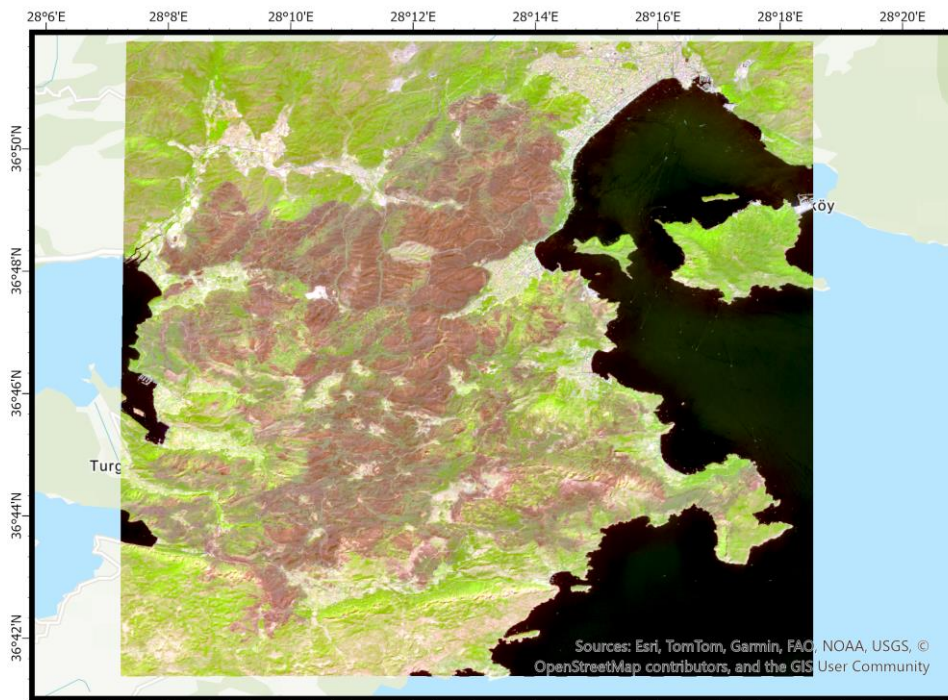


Figure 2.3. Sentinel-2 satellite image acquired on August 27, 2021 after the fire in the study area MR. The spectral bands B11, B8, and B4 displayed in red, green and blue color planes discriminate between the burned areas and unburned land cover.

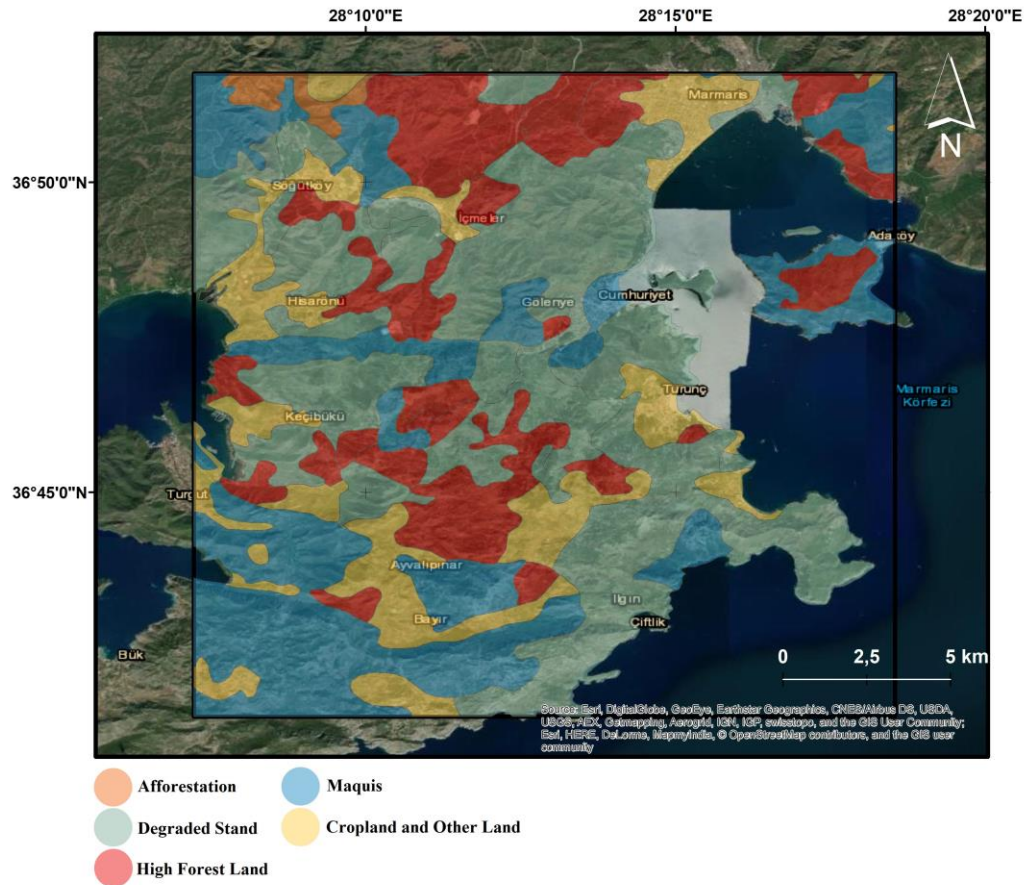


Figure 2.4. MR management plan according to LULC

Table 2.1. MR management plan according to LULC and tree species on hectare base

Management plan LULC	Tree Species	Area (ha)	%
Afforestation	Red pine	273.8	1
Degraded stand	Red pine	9337.2	39
High Forest land	Red pine	4785.5	20
Maquis	Maquies vegetation	6093.6	25
Cropland and other land	-	3718.7	15

Study Area – KV: This study area is located within the borders of Muğla province of Türkiye. The size of the selected area is about 64285,73 ha, including the burned forest areas and is shown in Figure 2.5. Based on the ESA WorldCover, this study area in 2021 includes 52388.2 ha of trees, 1679.9 ha of shrubland, 7022.9 ha of grassland,

1894.8 ha of cropland, 292.6 ha of built-up, 1000 ha of barren/sparse vegetation, and 14.4 ha of open water. In this area, the dominant tree species are red pine and black pine. Of the forest area, 13% is degraded stand, 46% is high forest land and 15% includes Maquis vegetation (Figure 2.6 & Table 2.2). Based on the Köppen-Trewartha climate classification, the region has a subtropical dry summer climate, and Mediterranean climate. In this area, the forest fire started on August 2, 2021 and after 6 days, it was brought under control on August 8, 2021. The majority of the burned area is a qualified forest asset. Cropland and settlement areas are quite small.

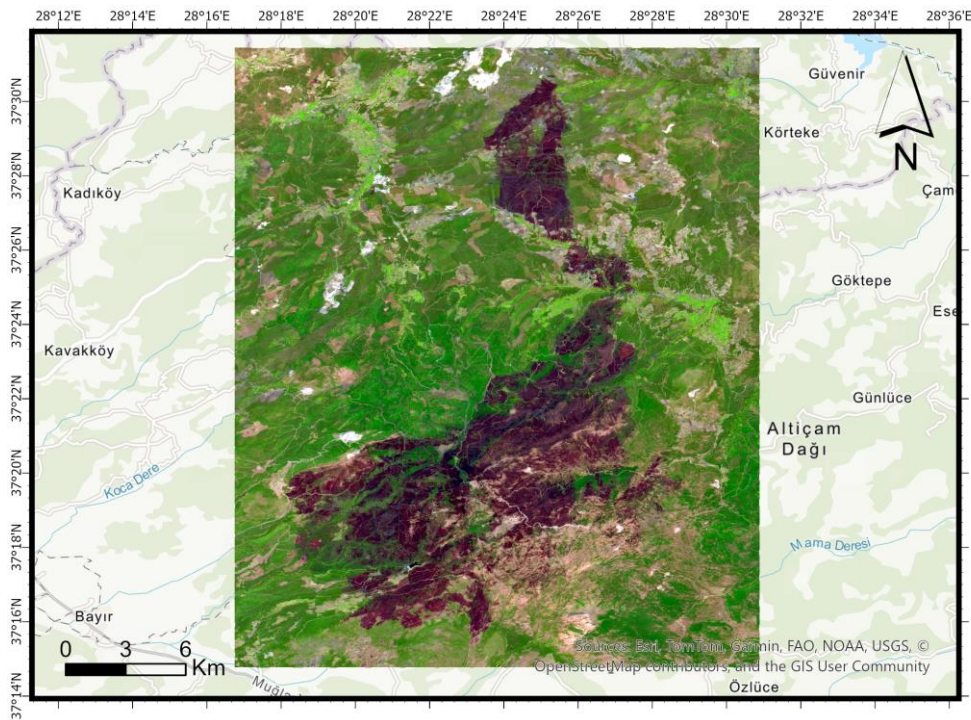


Figure 2.5. Sentinel-2 satellite image acquired on August 17, 2021 after the fire in the study area KV. The spectral bands B11, B8, and B4 displayed in red, green and blue color planes discriminate between the burned areas and unburned land cover.

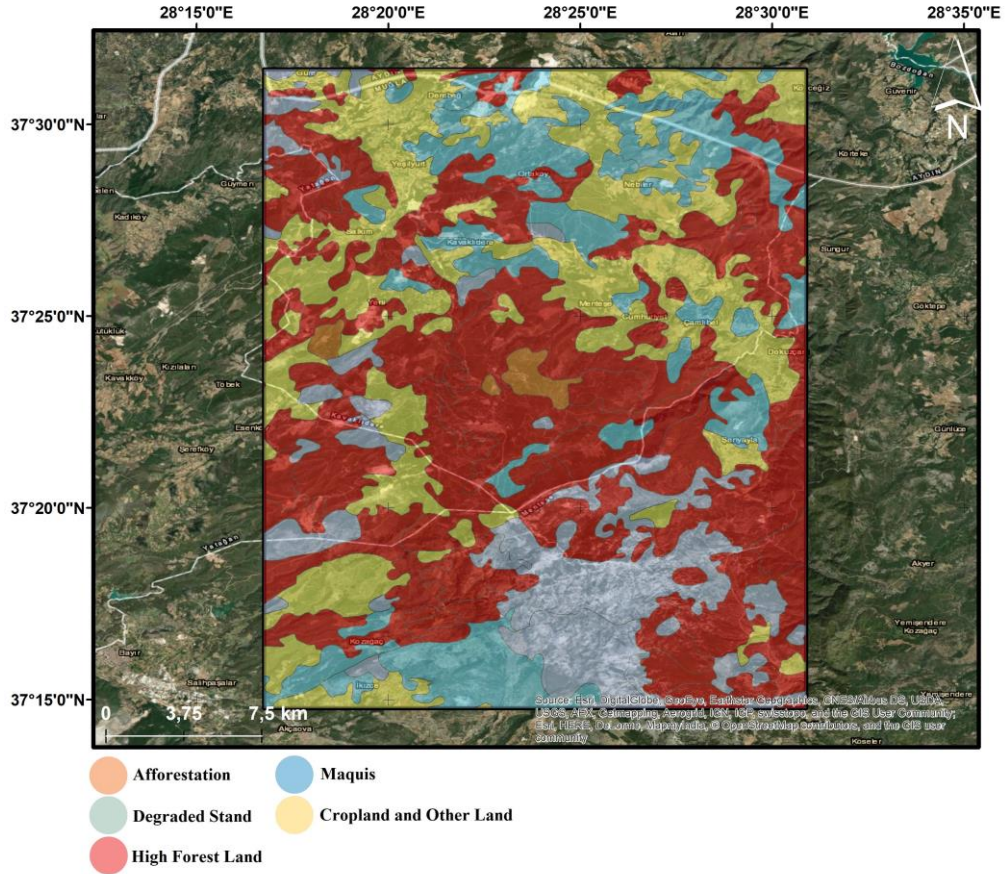


Figure 2.6. KV management plan according to LULC.

Table 2.2. KV management plan according to LULC and tree species on hectare base.

Management plan LULC	Tree Species	Area(ha)	%
Afforestation	Red pine	647.1	1
Degraded stand	Red pine + Black pine	8588.2	13
High Forest land	Red pine + Black pine	29351.8	46
Maquis	Maquies vegetation	9706.9	15
Cropland and other land	-	15964.6	25

Study Area -MG: This area is located within the borders of Antalya province of Türkiye. The size of the selected area is about 161177,11 ha, including the burned forest areas and is shown in Figure 2.7. Based on the ESA WorldCover, the area in 2021 includes 94048.1 ha of trees, 11293.1 ha of shrubland, 30544.1 ha of grassland, 9217.2 ha of cropland, 3427 ha of built-up, 1877.3 ha of barren/sparse vegetation, 10712.3 ha

of open water, and 57,8 ha of herbaceous wetland (Figure 2.8 & Table 2.3). In this area the dominant tree species are red pine, black pine and partly juniper. There are small amounts of oak, beech and hornbeam in forest areas. Of the forest area, 13% is degraded stand, 31% is high forest land, 7% includes Maquis vegetation and 13% includes degraded coppice. According to the long-term measurements of the General Directorate of Meteorology, the yearly average temperature of Antalya province is 18.8°C, the yearly average maximum temperature is 24.2°C, and the yearly minimum temperature is 13.8°C. The average monthly total rainfall is 1053.4 mm. According to the Köppen-Trewartha climate classification, the region has a subtropical dry summer climate, and Mediterranean climate. In this area, forest fire started on July 28, 2021 and was brought under control on August 8, 2021. The fire damaged an intensive cropland area along with the forest area.

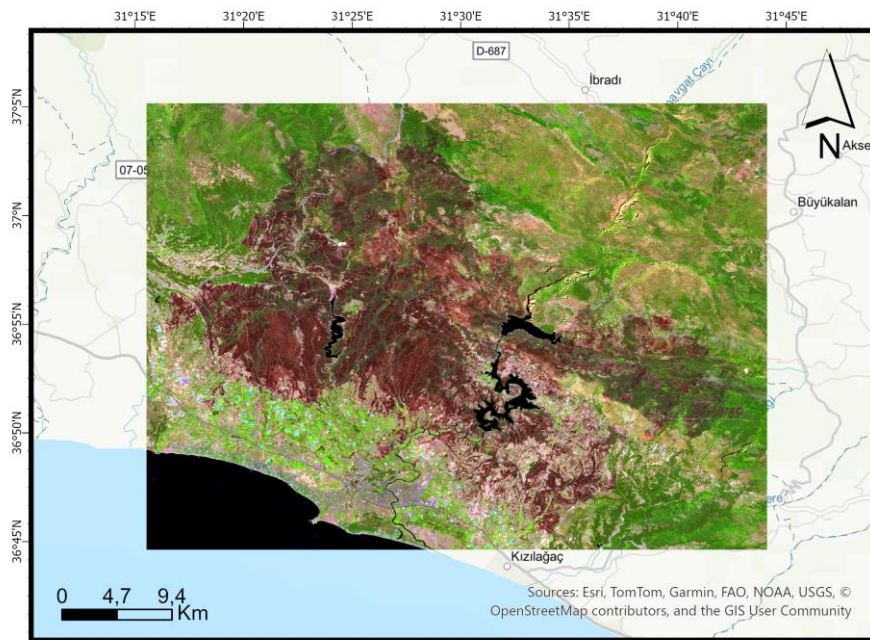


Figure 2.7. Sentinel-2 satellite image acquired on August 09, 2021 after the fire in the study area MG. The spectral bands B11, B8, and B4 displayed in red, green and blue color planes discriminate between the burned areas and unburned land cover.

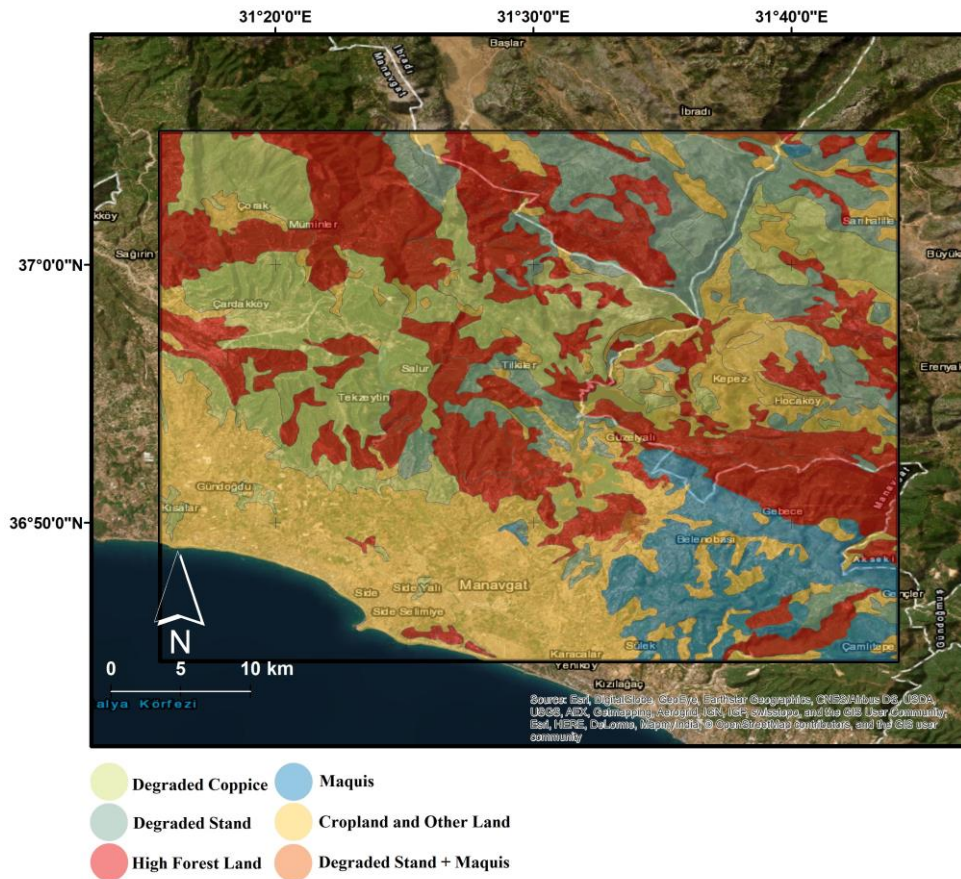


Figure 2.8. MG management plan according to LULC.

Table 2.3. MG management plan according to LULC and tree species on hectare base.

Management plan LULC	Tree Species	Area(ha)	%
Degraded coppice		28509.8	19
Degraded stand	Red pine + Juniper +Oak	19761.9	13
Degraded forest land + Maquis	Red pine + Juniper + Maquies vegetation	493.4	1
High Forest land	Red pine + Black pine + Juniper	47103.1	31
Maquis	Maquies vegetation	11521.6	7
Cropland and other land		45449.1	29

Study Area 4 – CK: This study area is located within the borders of Çanakkale province of Türkiye. The size of the selected area is about 36922,25 ha, including the burned forest areas and is shown in Figure 2.9. Based on the ESA WorldCover, the study area

in 2021 includes 18044.8 ha of trees, 1353 ha of shrubland, 6109.6 ha of grassland, 7861 ha of cropland, 1159 ha of built-up, 176.9 ha of barren/sparse vegetation, 2176 ha of open water, and 42.1 ha of herbaceous wetland. In this study area, the dominant tree species is red pine. Of the forest areas, 17% are degraded stand, 37% are high forest land. Among the four study areas used this study area contains the most intensive cropland with 46% (Figure 2.10 & Table 2.4). According to the long-term measurements of the General Directorate of Meteorology, the yearly average temperature of Çanakkale province is 15.2°C, the yearly average maximum temperature is 19.7°C, and the yearly minimum temperature is 10.9°C. The average monthly total rainfall is 625.3 mm. According to the Köppen-Trewartha climate classification, the region has a subtropical dry summer climate, and Mediterranean climate. Two forest fires have recently occurred within the boundaries of the study area in the same year. The first forest fire occurred on July 16, 2023 and was brought under control after 52 hours. The second forest fire started on August 22, 2023 and was taken under control on August 24, 2023. In addition to the forest areas, agricultural lands were also damaged by the fire.

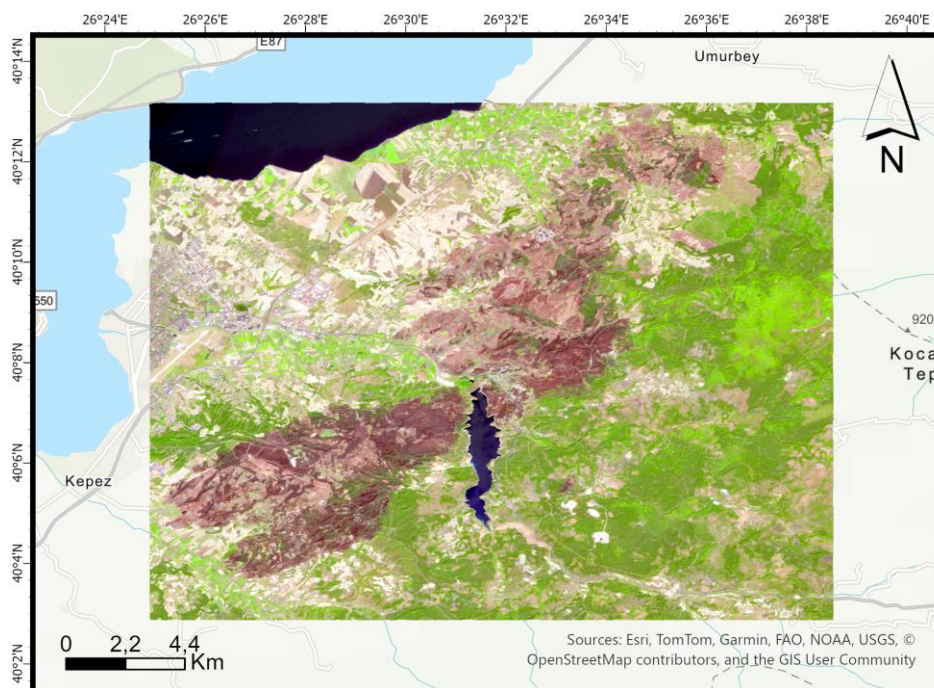


Figure 2.9. Sentinel-2 satellite image acquired on August 28, 2023 after the fire in the study area CK. The spectral bands B11, B8, and B4 displayed in red, green and blue color planes discriminate between the burned areas and unburned land cover.

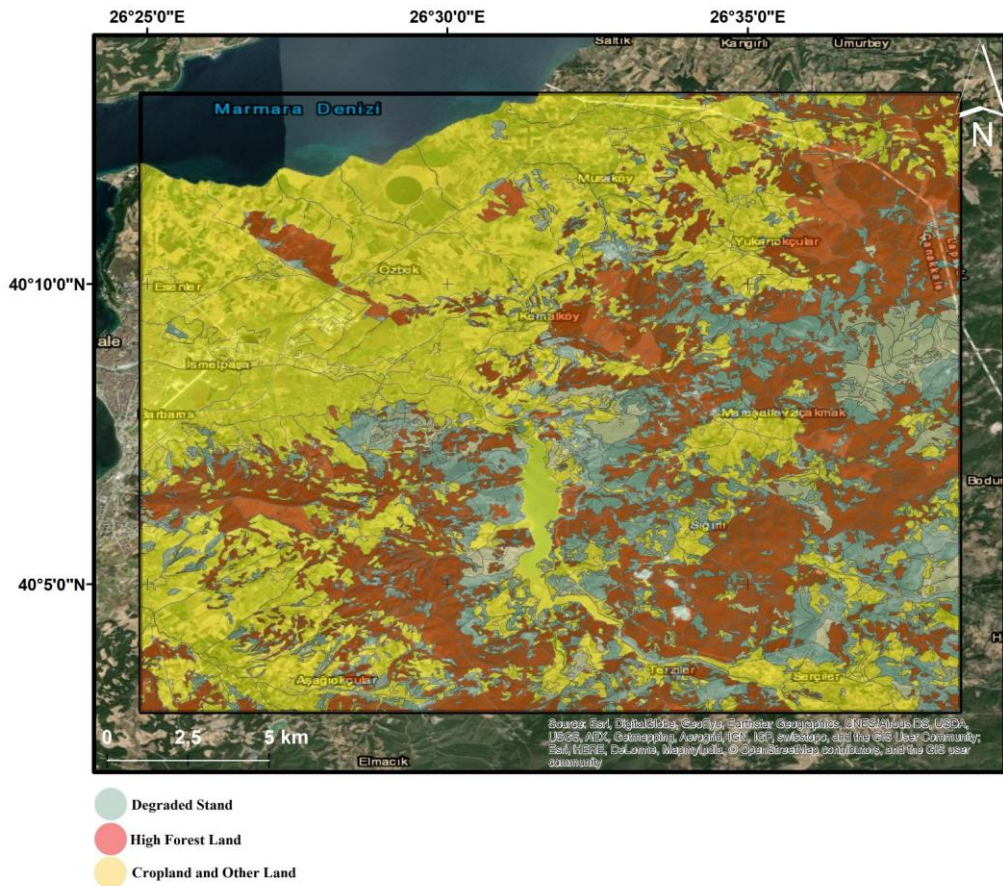


Figure 2.10. CK management plan according to LULC.

Table 2.4. CK management plan according to LULC and tree species on hectare base.

Management plan LULC	Tree Species	Area(ha)	%
Degraded stand	Red pine	5970.25	17
High Forest land	Red pine	12994.08	37
Cropland and other land		16154.80	46

2.2. Data

2.2.1 Sentinel-2 MSI Images

Sentinel-2 is a 13-spectral-band, wide-area, high-resolution, multi-spectral imaging mission developed by the ESA. It is based on two identical satellites orbiting each other. Sentinel-2 has a MSI sensor with 13 spectral bands ranging in size from 10 to 60-meter pixels. The orbital swath is 290 km, and the twin satellites in the same orbit aim to provide a high equatorial revisit frequency of 5 days [58]. The spatial and spectral characteristics of Sentinel-2 MSI sensor is given in Table 2.5.

Table 2.5. Sentinel-2 MSI Bands.

Band	Resolution (m)	Central Wavelength (nm)	Description
B1	60	443	Ultra Blue (Coastal and Aerosol)
B2	10	490	Blue
B3	10	560	Green
B4	10	665	Red
B5	20	705	Visible and Near Infrared (VNIR)
B6	20	740	Visible and Near Infrared (VNIR)
B7	20	783	Visible and Near Infrared (VNIR)
B8	10	842	Visible and Near Infrared (VNIR)
B8a	20	865	Visible and Near Infrared (VNIR)
B9	60	940	Short Wave Infrared (SWIR)
B10	60	1375	Short Wave Infrared (SWIR)
B11	20	1610	Short Wave Infrared (SWIR)
B12	20	2190	Short Wave Infrared (SWIR)

The ortho-images of Level-1C (L1C) and Level-2A (L2A) tiles are 110x110 km² in UTM/WGS84 projection. Earth is split using a 100 km step and a predetermined set of tiles that are defined in UTM/WGS84 projection. GEE offers both L1C and L2A products. The L2A product offers atmospherically corrected surface reflectance images, which are derived from the L1C products. L2A items have been produced consistently

at the ground segment in Europe since March 2018, and manufacturing was expanded to the worldwide market in December 2018 [58].

In this study, Sentinel-2 L2A products with the ID 'COPERNICUS/S2_SR' in GEE were used. The satellite images used in the study are given in the Table 2.6.

Table 2.6. The Sentinel-2 images used in this study.

Study Area	Post-fire Images	Acquisition Date
MR	COPERNICUS/S2_SR/20210827T084601_20210827T090001_T35SPA	2021-08-27
KV	COPERNICUS/S2_SR/20210817T084601_20210817T085325_T35SPB	2021-08-17
MG	COPERNICUS/S2_SR/20210809T083559_20210809T083843_T36SUF COPERNICUS/S2_SR/20210809T083559_20210809T083843_T36SUG	2021-08-09
CK	COPERNICUS/S2_SR/20230828T090559_20230828T091557_T35TME	2023-08-28

Previous studies have demonstrated that the near infrared (NIR) and short-wave infrared (SWIR) bands are sensitive to fire effects [14, 54, 59-61]. When leaves are burned, fire causes a decrease in leaf area index and a reduction and drying of leaf pigment. The first effects after fire are usually observed as a decrease in NIR reflectance, while dryness causes an increase in SWIR reflectance [14]. Little sensitivity to fire has been detected in the visible bands, but it has been used in studies to mask clouds and reduce confusion about cultivated areas [62]. Based on the scope of these studies, the bands B2, B3, B4, B8, B11, and B12 were used in this study (Table 2.7.).

Table 2.7. The Sentinel-2 MSI bands used in this study.

Band	Description	Resolution (m)
B2	Blue	10
B3	Green	10
B4	Red	10
B8	NIR	10
B11	SWIR 1	20
B12	SWIR 2	20

2.2.2. Ancillary Data

The performance of the proposed methodology was evaluated by comparing the detected burned areas with the burned areas available in national and global burned area data sets. The purpose of this comparison was not to verify the methodology employed in the study, but to reflect the differences and uncertainties of the burned areas information between different global and national data sets. For this purpose, General Directorate of Forestry Data was used as the national burned area dataset, and Copernicus Climate Change Service (C3S) - C3SBA10 and MODIS - MCD64A1 and European Forest Fire Information System – EFFIS were used as the global burned area data sets.

General Directorate of Forestry Data; The GDF is a public institution with a distinct budgetary and legal status which is affiliated with the Ministry of Agriculture and Forestry. Protecting forests and forest resources, managing and developing forests in a sustainable manner within the integrity of the ecosystem and providing multifaceted benefits to society are among the duties and responsibilities of the GDF. GDF keeps the information about the burned forest areas statistically, on a hectare basis, on the date and time of fire outbreak and the amount of burned area, specific to the regional directorate, operation directorate, operation chief, province and district. The data obtained from GDF and used for comparison in this study are not spatial data.

Copernicus Climate Change Service (C3S) - C3SBA10; C3S's burned area product named C3SBA10 offers two burned area products at different spatial resolutions in pixel and grid scale. Burn area product was produced by analysis of reflectance changes from MODIS Terra and Sentinel-3 OLCI medium resolution sensors [63]. Product outputs are provided to users free of charge in NetCDF4 format, at 300 m spatial resolution for pixel products and 0.25° spatial resolution for grid products [64]. In this study, the 300 m spatial resolution pixel product of the C3SBA10 burn area product was used to compare with other data. Since the data used was provided for the period 2017-2022, a comparison was made for the MR, KV, MG study areas. A comparison could not be made for the C3SBA10 burn area product for the CK area, where the forest fire occurred in 2023.

MODIS - MCD64A1; The MODIS-MCD64A1 burned area product served on a global scale is a 500-meter (m) product with a spherical grid containing burned area information per pixel. The MCD64A1 product integrates 1 km MODIS active burned area observations and 500 m MODIS Surface Reflectance images [65]. MCD64A1 product creates a fire-sensitive spectral band index with red, near-infrared and short-wave infrared bands. Then, MODIS applies dynamic thresholds to Terra and Aqua images and serves burned area data at monthly temporal resolution from 2000 to the present [66].

European Forest Fire Information System – EFFIS; EFFIS, supports services against fire protection of forests in the European Union and neighboring countries and provides up-to-date and reliable information. The system is one of the components of Copernicus-Emergency Management Services [57]. EFFIS is obtained by integrating burned area data, MODIS VNIR (250 m) and MODIS SWIR (500 m) and MODIS active fire product (1 km) data and various auxiliary data [66, 67]. In addition, the entire process is integrated with visual image interpretation and systematic analysis of news from various media sources [68]. The main task of the system is to provide a daily fire risk map for EU countries and to map forest fires larger than 50 hectares [67]. Burned area information in the EFFIS database is mainly obtained from forests. Burned areas seen in areas such as agricultural areas and cultivated areas are not included in this database. In the EFFIS database, information is kept in vector data format and is offered to users free of charge [66].

3. METHODOLOGY

Figure 3.1 shows the general steps of the methodology employed in this study to detect/map burned forest areas through object-based image classification from uni-temporal Sentinel-2 imagery based on GEE and code editor platform and to evaluate the spatial and temporal transferability of the RF algorithm. The first step includes the pre-processing and preparations of the data for the analysis. Step 2 includes image segmentation and object-based classification. The last step, step 3, involves model transferability and evaluation of the results.

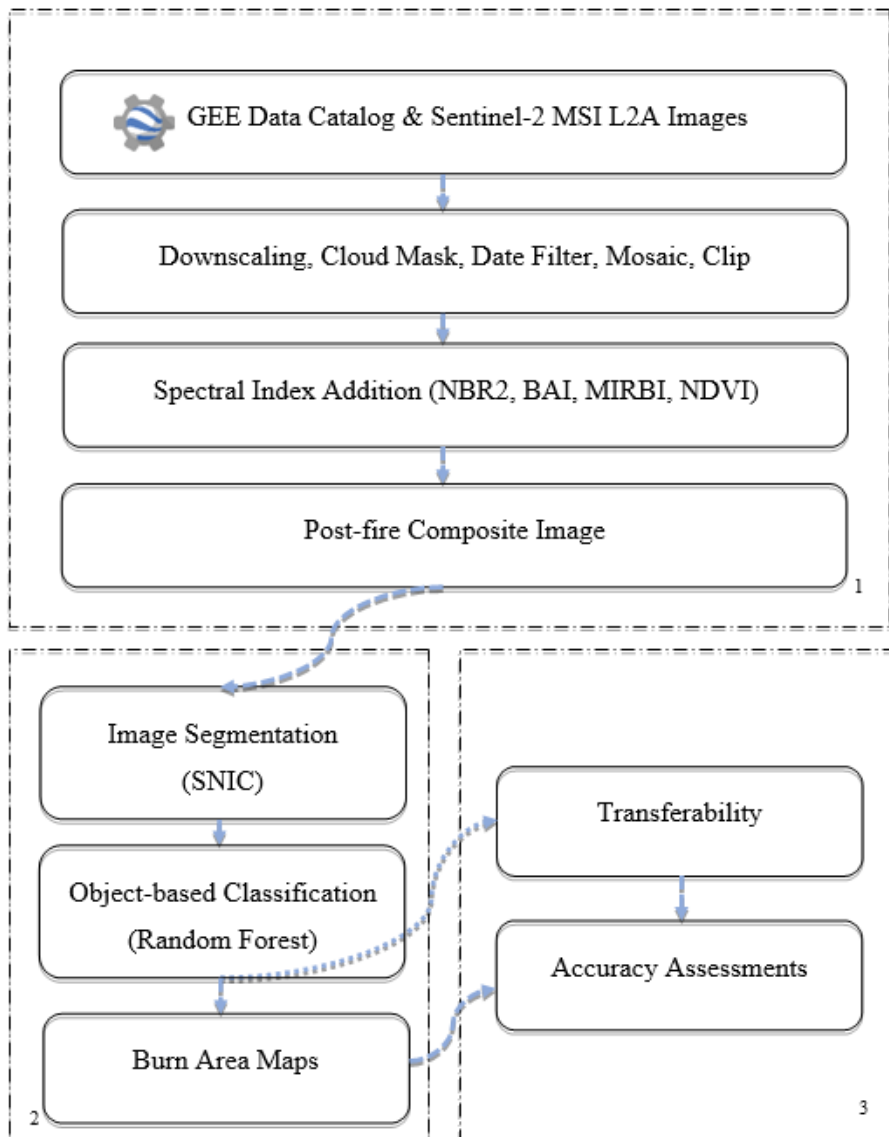


Figure 3.1. Workflow of the methodology

3.1. Software Used

GEE platform was used for all operations in step 1 and step 2 and for the “transferability” part in Step 3 in Figure 3.1. This corresponds to a large part of the proposed methodology. GEE is a scientific research and visualization tool for geographic datasets used by academics, non-profits, businesses, and governments. GEE hosts satellite imagery and preserves it in a public data library that includes earth images extending back over four decades [69]. The GEE Data Catalog is a comprehensive repository of geospatial datasets available within the GEE platform. The platform offers users access to a comprehensive array of Earth observation data, encompassing satellite imagery, climate data, land cover maps, terrain data, and other related resources.

Key features of the GEE Data Catalog include the followings: the catalog that provides detailed metadata for each dataset, including descriptions, spatial and temporal resolutions, citation information, and access permissions. Users can import datasets directly into their GEE scripts and workflows, allowing for seamless integration with GEE's analysis tools and computing resources [69]. GEE leverages Google's cloud infrastructure to provide scalable computing resources for processing and analyzing large geospatial datasets. Users can write and execute code using the GEE JavaScript API or Python API directly in their web browser or through integrated development environments (IDEs) like Google Colab [70].

GEE also provides tools and functions for performing various geospatial analysis tasks, including image classification, change detection, time series analysis, and spatial modeling. Users can apply algorithms to process and analyze imagery, extract information, and generate insights about land cover, land use, vegetation dynamics, and more. Furthermore, GEE offers interactive visualization capabilities that allow users to explore geospatial datasets and analyze results through dynamic maps, charts, and graphs [71]. At the present time, applications based on Landsat, Modis and Sentinel imagery for burned area mapping are performed using GEE [72, 73].

For the “accuracy assessment” part in Step 3, the ArcGIS Pro 3.2 software and Google Earth Pro software were used. For accuracy assessment, the ‘Create Accuracy Assessment Points’ tool in ArcGIS Pro software was used to assign points to the study areas by stratified random sampling method. Google Earth Pro software was used for visual interpretation with high resolution data. After all points were evaluated, the ‘Compute Confusion Matrix’ in ArcGIS Pro software was used to create the confusion matrix and obtain the accuracy.

3.2. Sentinel-2 Data Preprocessing and Spectral Indices

The preprocessing operations carried out on the Sentinel-2 data include image clipping and mosaicking, and cloud masking on the post-fire satellite imagery used. In addition, in order to ensure that all spectral bands used in this study have the same geometric resolution, 20 m resolution bands were resampled to 10 m resolution using the bicubic interpolation method. The ‘ee.Image.resample’ function of GEE was used for this step.

Several spectral indices were computed from the spectral bands of Sentinel-2 and used as additional bands in the classification. In the study conducted by [55], spectral sensitivity analysis was performed with the objective of determining which bands and/or spectral indices are the most suitable ones for burn area detection from Sentinel-2 images. Spectral sensitivity analysis was performed with parametric/non-parametric analyses and the performances were compared. In the study conducted by [74] post-fire Sentinel-2 images were used to select burned and unburned adjacent areas of different land cover types and the separability index was employed to quantify the degree of separability between the areas with the performance of the indexes was evaluated. Therefore, inspired from these studies the mid-infrared burn index (MIRBI), burn area index (BAI), normalized burn ratio 2 (NBR2), and normalized difference vegetation index (NDVI) were selected as the spectral indices (Table 3.1.).

Table 3.1. Spectral indices used in this study

Spectral Index	Equation	References
MIRBI	$10 \times SWIR2 - 9.8 \times SWIR1 + 2$	[75]
BAI	$BAI = \frac{1}{(0.1 + R)^2 + (0.06 + NIR)^2}$	[76]
NBR2	$\frac{SWIR1 - SWIR2}{SWIR1 + SWIR2}$	[55]
NDVI	$NDVI = \frac{NIR - R}{NIR + R}$	[77]

Mid-infrared burn index (MIRBI): This index was developed especially for shrub ecosystems. It combines two Short Wave Infrared (SWIR) bands, which provides better spectral separation in burned areas and is suitable for assessing the effects of fire on vegetation, especially on shrub vegetation [75, 78].

Burn area index (BAI): It identifies areas affected by fire using red band (R) and NIR reflectance. This index stages the burned areas in the post-fire image with a charcoal black signal [76, 79].

Normalized burn ratio 2 (NBR2): This index modifies the NBR index to emphasize water sensitivity and uses the SWIR band instead of the NIR band [55, 79].

Normalized Difference Vegetation Index (NDVI): NDVI is related to vegetation monitoring and is widely used as the detection of burned areas [77, 79, 80].

3.3. Image Segmentation

Pixel-based approach has limitations in classifying images from optical images in terms of landscape texture, structure and shape and causes salt and paper noise in the classified image. Object-based image classification uses color, shape and topological

features of the image to classify the image into meaningful objects and then analyses and classifies these objects [34].

Object based image analysis (OBIA) consists of two main stages: segmentation and classification [81]. Segmentation is a crucial step in OBIA to divide pixels with similar properties and create homogenous picture objects [37]. The purpose of segmentation is to divide the image into meaningful objects according to features such as texture, color, shape, size and gray level [82]. Segmentation methods can be categorized as edge-based methods, region based methods, hybrid methods, and semantic methods [82]. The segmentation preferences to be used for segmentation are very important as they form the basis of the object-based classification process [83].

GMeans, KMeans and SNIC are three algorithms that can be used for image segmentation in GEE. In this study, SNIC algorithm was chosen as the segmentation algorithm. The SNIC algorithm is a non-iterative version of the simple linear iterative clustering (SLIC) algorithm [84]. It improves computational efficiency and segmentation quality, requires less memory and is a faster and simpler algorithm [84]. Similar to SLIC algorithm, it initializes the center points with pixels selected in the normal grid. Then, normalized spatial distances and color distances are used to determine the proximity of a pixel to the center. This creates homogeneous super pixels and the smallest distance from the center determines the candidate pixel to be selected [84]. Seed size, compactness, connectivity, and neighborhood size are the basic parameters of the SNIC algorithm in GEE. The compactness parameter affects the shape of the clusters, and higher values will result in more compact clusters, that is, closer to square. The connectivity parameter can be set as 4 or 8, and expresses how neighboring pixels will be taken when assigning them to the super pixel. The neighborhood size parameter specifies the window size used for clustering. The seed size parameter defines the super pixel seed location spacing in pixels [37, 44, 84-87].

The outputs of the SNIC algorithm vary depending on visualization scale on the GEE platform. It was therefore necessary in the code to use the "reproject" function to fix a proper output scale for the clusters. A regular seed grid was used using the

"Image.Segmentation.seedGrid" function of GEE for superpixel seed location. This affects the number of clusters. The most appropriate parameter value was found based on several trials. Considering the characteristics and sizes of the study areas, the parameter values were selected as follows: "seedGrid" = 50, "compactness" = 0, "connectivity" = 8, "neighborhoodSize" = 128. The SNIC algorithm implemented in GEE environment generates a multi-band raster dataset that consists of segments with the mean values computed for all bands of the input image, as well as a band that consists of the identification numbers assigned to the generated segments. In this way, for each segment, the mean value is calculated and all pixels that fall within a segment are assigned the mean value of the corresponding segment. The segmented image that contains the mean values of the image segments is then used as the input dataset for the classification operation.

3.4. Training Data

One of the main aims of this study was to evaluate the spatial and temporal transferability of the object-based ML classification algorithm. RF ML algorithm was selected as the classification algorithm. The algorithm was trained on the cloud-based GEE platform and its transferability was also tested. For this reason, each study area was trained with different training data and classified with two different RF models.

The training samples were collected based on the segments generated. In the GEE platform, the classifier is standardized on a pixel basis [88]. For this reason, for each segment the SNIC algorithm calculated the mean value from the pixels that fall within the segment, and all pixels falling within a segment were assigned the computed mean value of that segment [86]. First of all, 5%-20% of the number of segments from the segmented study areas were selected individually as the training segments using the geometry tools of the GEE web-based code editor. Training data were collected for two classes: 'burned' and 'unburned'. Training data was collected as feature collection and it has a property that stores the class label and properties that store the predictor variables. Then, the selected training samples were randomly split as training and validation in a ratio of 70 percent to 30 percent. The data allocated for training were used to train the model. Thus, a trained RF model was created for each study area using

the training data collected within it, and object-based classification was carried out using this model.

To evaluate the transferability of the RF model, the study areas were divided into target domain and source domain. Study areas MG and CK were selected as source domain and the RF model was trained with the data collected from these two domains. The reason for choosing these two study areas as source domain is that they contain a combination of forest types, diversity of land use classes and different topographic conditions, although they have the characteristics of Mediterranean forests, and the forest fires that occurred in these areas occurred in different years (in 2021 for MG and in 2023 for CK). Detailed description about the study areas is given in Chapter 2.2.1. All study areas (MR, MG, KV, CK) including MG and CK were used as the target domain. Figures 3.2, 3.3, 3.4, and 3.5 respectively show the locations of training samples collected from the study areas MR, KV, MG, and CK for the classes ‘burned’ and ‘unburned’.

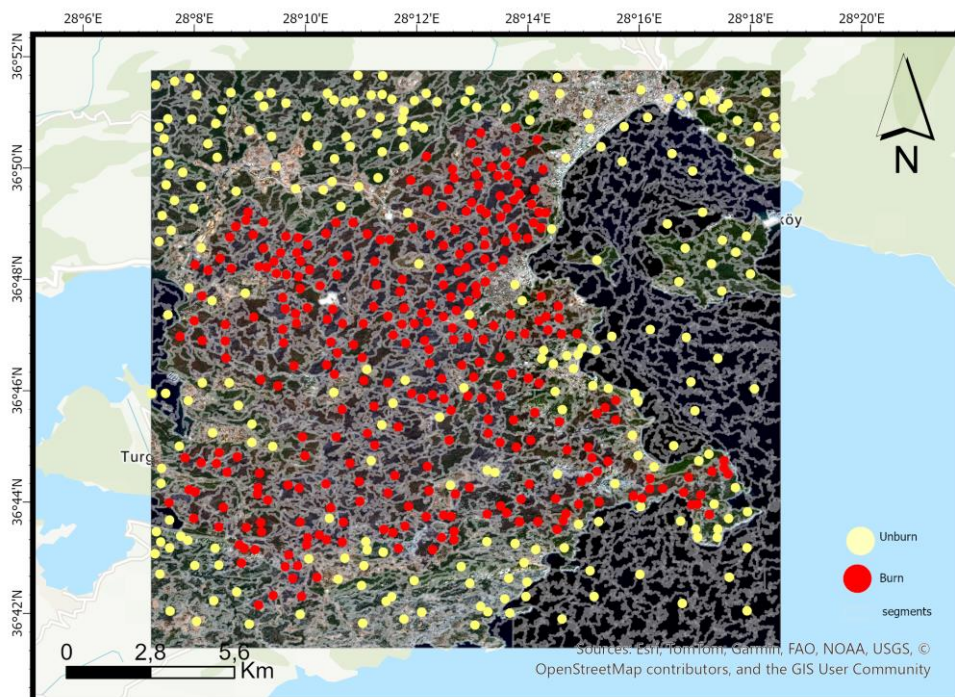


Figure 3.2. MR Study Area Training Data Set

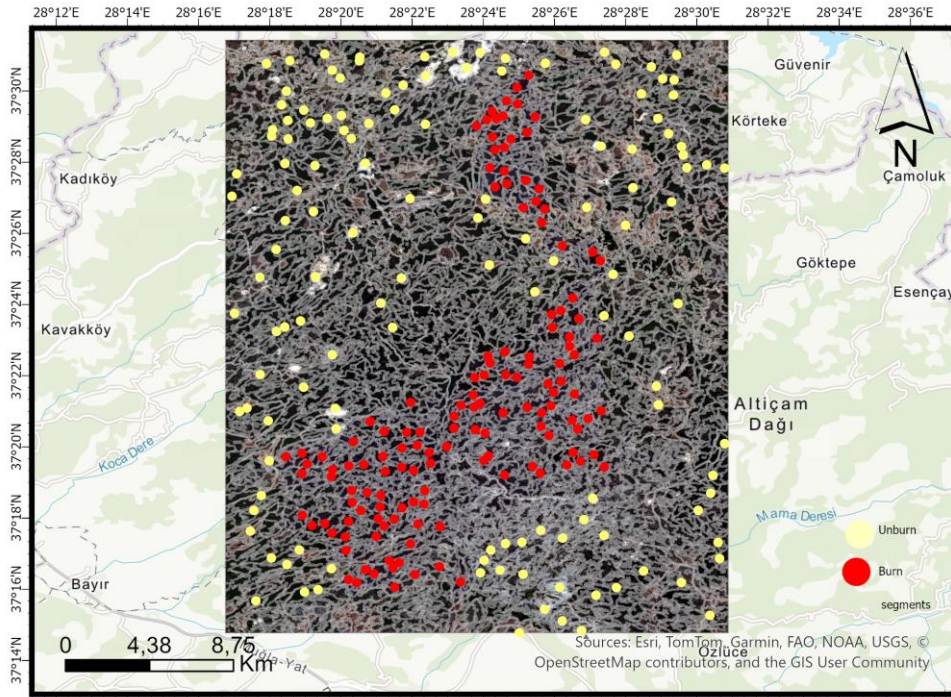


Figure 3.3. KV Study Area Training Data Set

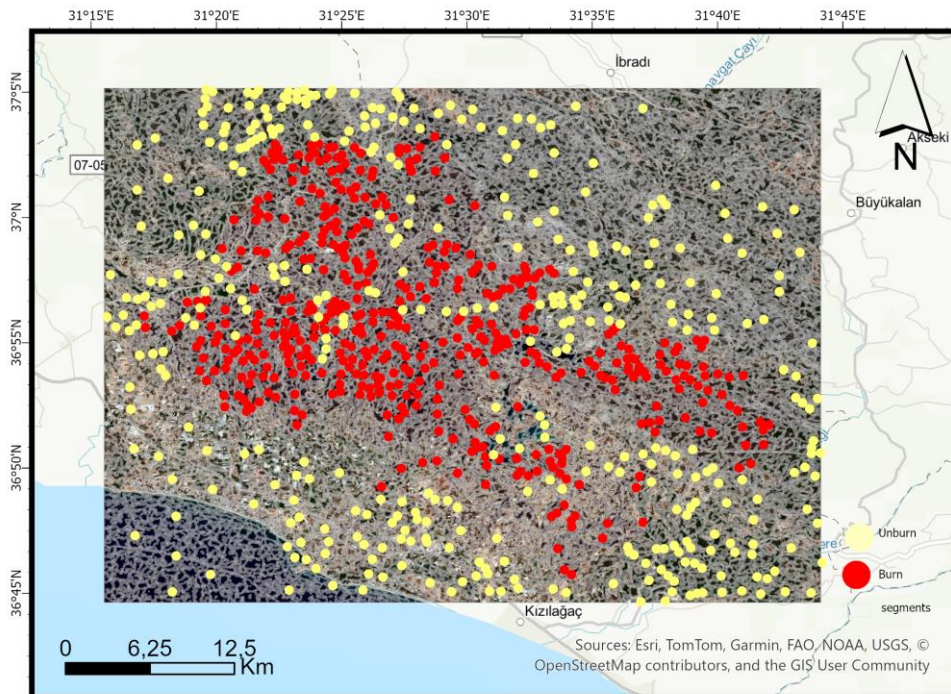


Figure 3.4. MG Study Area Training Data Set

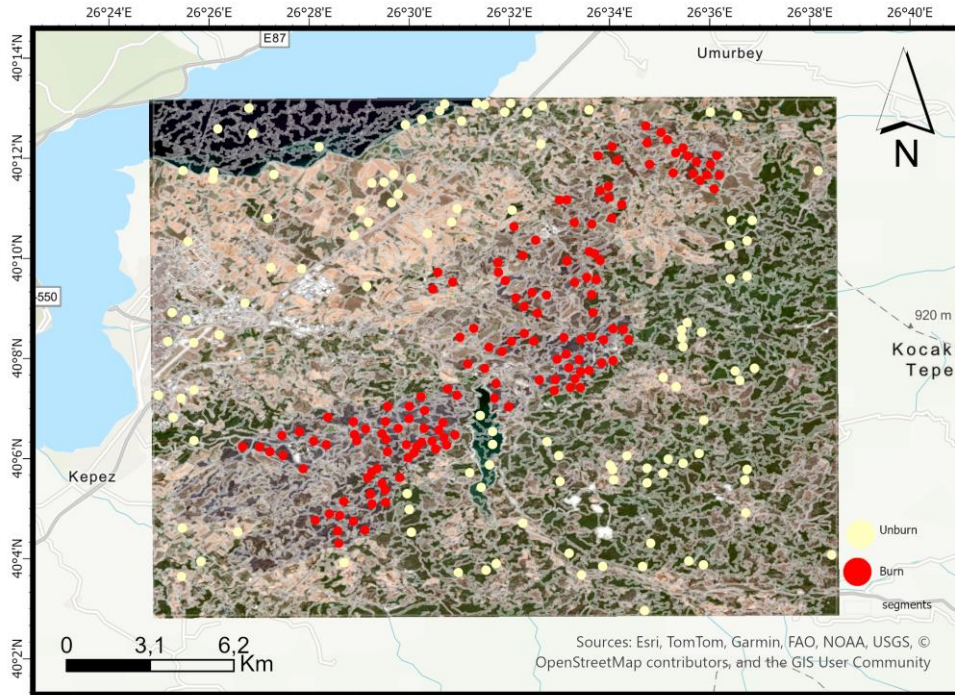


Figure 3.5. CK Study Area Training Data Set

3.5. Object-Based Classification

Despite the great advantages of remote sensing, especially in earth observation, various problems have been encountered in the detection of burned forest areas with satellite images. One problem is that multispectral reflectance creates various types of confusion. For example, mixing of lightly burned areas with other areas, especially shadows, bare soil, and water bodies, mixing of spectral reflections of burned areas and shaded areas can be given as examples. Object-based image analysis is an approach that uses spatial information as well as spectral information [42]. The fact that object-based classification uses color, shape, size and topological features of the image and thus analyses the objects and then proceeds to the classification stage provides a solution to many problems encountered in pixel-based classification.

In this study, image classification was carried out using an object-based approach. RF machine learning model was selected as the classification algorithm. For image

segmentation, which is the first step of object-based classification, the SNIC algorithm was selected.

Developed by [89] RF is an ensemble learning technique. RFs are combinations of tree estimates where each tree is sampled independently and all trees depend on the values of a vector with the same distribution [89]. RF is an advantageous classification algorithm with its robustness against outliers and overfitting and its ease of use [90]. High accuracy and processing speed are two important main benefits of RF [91]. In RF, each tree is trained on different training sets using bootstrap aggregation and error estimation [92, 93].

The main steps of RF algorithm are as follows (Figure 3.6):

Step 1: Selection of random samples from training set.

Step 2: Creating a decision tree for each training data associated with the training data.

Step 3: Making predictions and voting for all trees in the forest.

Step 4: Selection of the prediction result with the maximum number of votes as the prediction result.

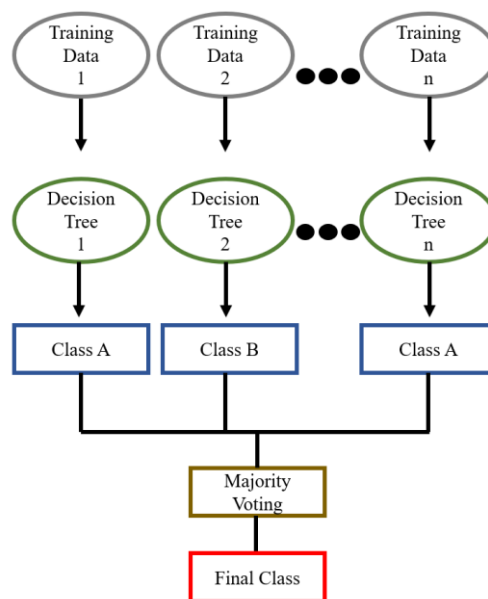


Figure 3.6. The RF Algorithm

In GEE, the ‘classifier’ package manages traditional ML algorithms, including RF. To implement RF in GEE several parameter values must be defined. These include “numberOfTrees”, the number of decision trees in the forest, “variablesPerSplit”, the number of variables per split, “minLeafPopulation”, the minimum leaf population, “bagFraction”, the bag fraction, the proportion of training data to be used in the creation of the next tree, “maxNodes”, the maximum number of nodes, and “seed”, the randomization seed.

Considering the number of classes used in this study (burned areas and unburned areas) 50 trees were built. The number of variables (bands) used for each split was computed as the square root of the number of the input bands.

3.6. Model Transferability

Transferability describes the situation where a model is trained on one partition and tested on another partition. Spatial transferability is the training of a model in one area and testing it in other areas. This method is relevant to remote sensing studies that deal with large geographical areas or different temporal scales. Evaluating the spatial and temporal transferability of ML algorithms, seeing the usability of the developed models in different areas and at different times, and testing their success is an important step to generalize the algorithms and classification results and to adapt them faster to future studies [40].

In the literature, model transferability has been applied to different satellite images of different resolutions with different scenarios to detect burned forest areas or to determine the fire severity in burned forest areas, and the transferability of the model has been successfully achieved spatially and temporally [36, 37, 39, 42, 43]. RF is a classification algorithm characterized by its robustness and adaptability to outliers [90]. This makes it a valuable tool for good generalization and adaptation to new datasets and conditions across different geographical regions and environmental conditions. Several studies have tested the transferability of the RF algorithm for mapping burned forest areas using Sentinel-2 imagery for different ecosystems and experimenting with

different scenarios. [39] tested the transferability of the RF algorithm for two different forest fires in South Korea with sentinel-2 images. [37] tested the transferability of the RF algorithm on the GEE platform with the object-based classification method and obtained successful results for South Korea. These studies show the potential of the transferability of the RF algorithm for mapping burned forest areas. This potential can accelerate and facilitate the process of mapping burned areas and the acquisition of spatial information and support opinion makers to make informed decisions.

One of the main objectives of this study was to assess the transferability of the object-based ML classification algorithm for burned area mapping using cloud computing and freely available Sentinel-2 images. This will enable a great potential for rapid damage assessment and the formulation of emergency response plans to be identified, without the need for pre-intervention for possible future forest fires specific to the Mediterranean forests, woodland and scrub biome.

To implement the concept of the model transferability, the study areas (4 in total) were divided into target domain and source domain. Study areas MG and CK were selected as the source domain as they are located in different geographical regions with different combinations of forest types, diversity of land use classes and topographic conditions. Furthermore, in these study areas the fire events occurred in different years. In study area MG, the fire event occurred in 2021, while in study area CK, the fire event occurred in 2023. Detailed description about the study areas are given in Chapter 2.2.1. The spatial, spectral and temporal characteristics of the study areas make the transferability of the object-based RF machine learning classification more challenging. The RF algorithm was trained using the samples collected from these two areas. Then, the trained model was applied to all study areas to map the burnt areas. In this regard, the present study aims to provide spectral diversity with the training data collected from two study areas and test the transferability of the model spatially and temporally by means of applying it in all study areas.

3.7. Accuracy Assessment

The accuracy assessment of the classified images is an important step in remote sensing studies, as it is an indicator of how well the classification objective is achieved and how well objects are extracted from the image. In order to evaluate the accuracy, validation data, usually called ground truth or reference data, are needed [94].

In this study, samples for ground truth were created using the natural color, false color band composites, and high-resolution Google Earth images. For each of the study areas CK and MR, 1000 points were selected, while for study areas KV and MG respectively, 1200 and 1500 points were selected using the ArcGIS Pro software (Table 3.2.). The sample selection procedure was based on the stratified random sampling method. Accuracy values were computed by comparing the classification results with the ground truth samples based on an error matrix. The tools used in ArcGIS Pro software are given in Chapter 3.1.

Table 3.2. The number of samples used for accuracy validation

Study Area	Ground Truth Samples
CK	1000
MR	1000
KV	1200
MG	1500

Error Matrix (EM) gives three accuracy measures, Producer's accuracy (PA), User's accuracy (UA) and Overall accuracy (OA). An EM is a square matrix expressing the number of pixels assigned to certain classes according to the reference data [95]. It is a suitable technique to communicate classification accuracy since it describes each class along with both the mistakes of inclusion (commission error) and errors of exclusion (omission error) [95]. OA is defined as the total number of correctly classified pixels (sum of diagonals) divided by the total number of reference pixels. PA is derived by dividing the number of successfully categorized pixels in each class by the number of sample data set pixels used for that class, and it represents how effectively the sampling

set pixels of a certain land cover type can be classified. The UA is the number of properly classified pixels within each class divided by the total number of pixels classified within that category, and it reflects how likely it is that a pixel assigned to a class represents that class.

The kappa coefficient found by [96] is also widely used in accuracy assessment. All elements in the error matrix are used to calculate the kappa coefficient. In this study, OA, PA, UA and Kappa coefficient values were calculated to assess the accuracy of the classified images.

4. RESULTS AND DISCUSSIONS

4.1. Segmentation

Segmentation was performed using a total of ten bands including six bands (B2, B3, B4, B8, B11, B12) of Sentinel-2 data and four spectral indices (MIRBI, BAI, NBR2, NDVI) derived from Sentinel-2 data. GEE creates a multiband raster dataset as an output after defining the SNIC segments, i.e., clusters. This multiband raster dataset contains the clusters and additional layers that contain the mean values of the input bands.

In this study, the input image is a 10-band composite image. The output of the SNIC algorithm is a 11-band raster dataset. Of these 11 bands, 10 bands contain the mean values of the input bands calculated for each segment from the pixels that fall within the segment. One band contains the clusters. With the segmentation step, similar pixels are grouped, reducing the number of input elements for the object-based classification process.

The SNIC segmentation generated a total of 2016 segments for study area MR, 4056 segments for study area CV, 10176 segments for study area MG and 2250 segments for study area CK. Hence, with the segmentation process, the input data elements (number of pixels) decreased from 4046526 to 2016 for study area MR, from 6425837 to 4046 for study area CV, from 20210553 to 10176 for study area MG and from 3689469 to 2250 for study area CK. Figure 4.1 shows the result of SNIC segmentation for study area MR. Figure 4.2 shows the result of SNIC segmentation in vector form for study area MR. Figure 4.3 depicts the result of SNIC segmentation for study area KV. Figure 4.4 depicts the result of SNIC segmentation in vector form for study area KV. Similarly, Figure 4.5 shows the result of SNIC segmentation for study area MG. Figure 4.6 shows the result of SNIC segmentation in vector form for study area MG. Figure 4.7 illustrate the result of SNIC segmentation of study area CK. Figure 4.8 shows the result of SNIC segmentation in vector form for study area CK.

Since the classifier in GEE is standardized on a pixel basis, in order to implement an object-based classification approach, the same brightness value, such as the mean value must be assigned to each pixel in a segment. The SNIC algorithm overcomes this problem by creating a multiband raster dataset with the mean bands. Since the SNIC output image varies depending on the visualization scale, the output scale should be fixed for clusters with segmentation outputs. In this study, the cluster output scales were fixed to Sentinel-2's native resolution of 10m. The output scale of the clusters affects the processing time. For example, setting the clusters to a lower scale was found to speed up the processing time.

The SNIC algorithm in GEE is based on a regularly spaced seed grid. The selected seed grid parameter, i.e. the superpixel seed position range in pixels, influences the number of clusters. The evaluation of different cluster shapes with varying seed grid parameters is necessary to find a more effective cluster size for the study area and size of the landscape patches. [86] compared different classification algorithms in terms of OA by applying various seed grid parameters to different data sets for LULC classification over Sentinel-2 and Landsat-8 images and emphasized that testing various seed grid parameters would be useful in finding the effective cluster size.

In this study, for each study area, the seed grid parameter value was determined based on several trials taking into consideration the heterogeneity of the study areas. Figure 4.9 shows the results of different seed grid parameters tried for a part of the MR study area. In order to avoid over and under segmentation procedures it is important to generate segments with appropriate sizes. Under segmentation results in more complex objects and an inherent error in classification [97]. Over-segmentation may be preferred to under-segmentation because it is a more complex process to split segments than to merge them [52]. In this study, the selected study areas are quite heterogeneous. Moreover, burned areas themselves are also heterogeneous as they tend to be burned with different severity. Thus, over-segmentation was preferred in this study. Figure 4.10 is an example that shows over-segmentation for a part of study area MR when the seed grid parameter is set to 50. Over-segmentation would generate higher number of

segments with smaller sizes. Although this increases the computation time for classification, it does not affect the classification accuracy [98].

The computation and analysis required for segmentation and object-based classification in GEE is computationally and analytically heavy, and this can lead to errors or longer time for the analysis due to the processing and memory limit quotas that GEE offers free of charge to the users [37]. Especially the conversion of the segments in raster form into vector form takes a long time if the seed grid parameter is kept low and the number of segments is high. In this study, the result of image segmentation was converted to vector form only for the visual analysis of the segments and to collect training samples from the segments. For the developed code to run fast and avoid problems due to over segmentation, all operations except training data collection were successfully carried out on raster dataset.

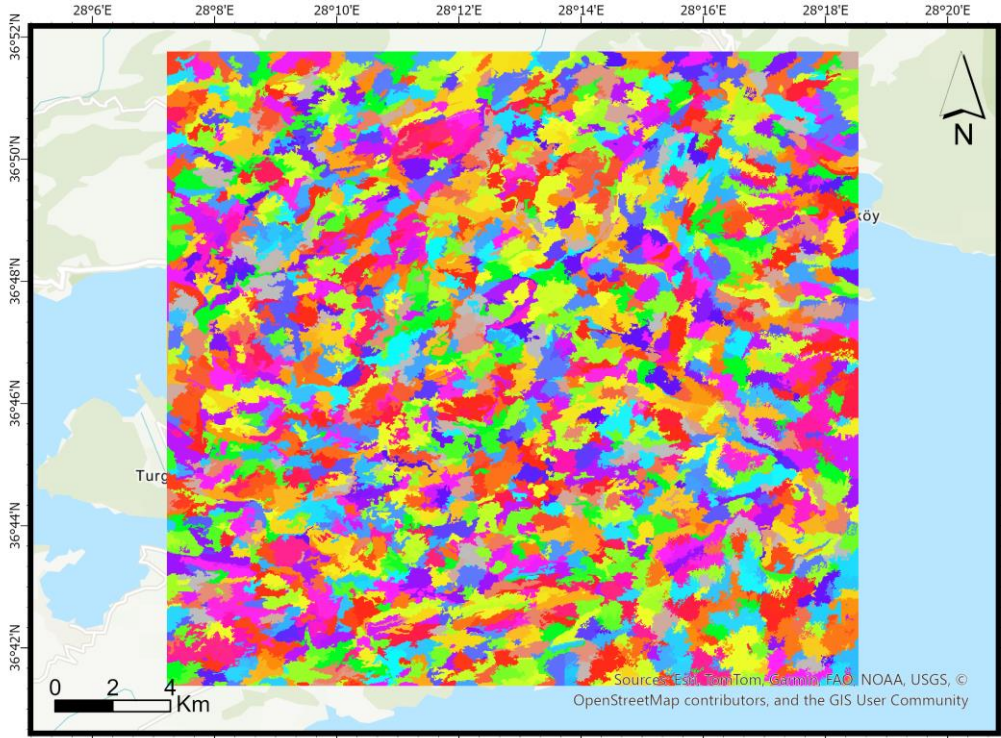


Figure 4.1. The result of SNIC segmentation for study area MR.

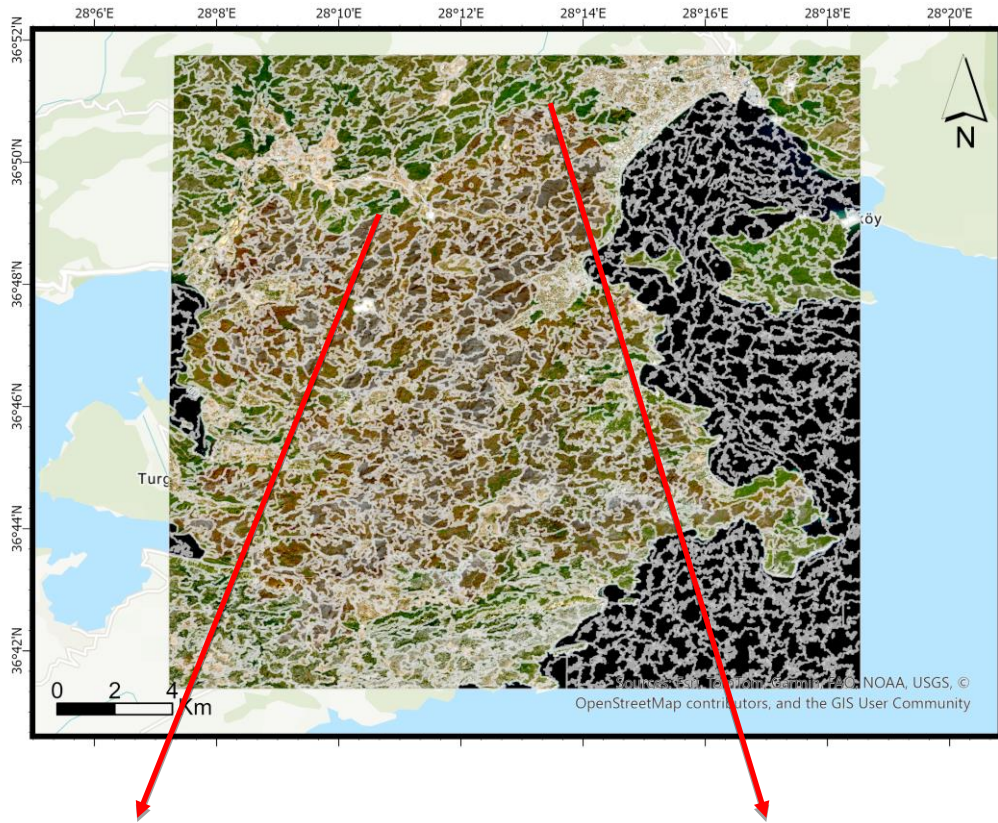


Figure 4.2. The segments in vector form for study area MR (Seed size: 50).

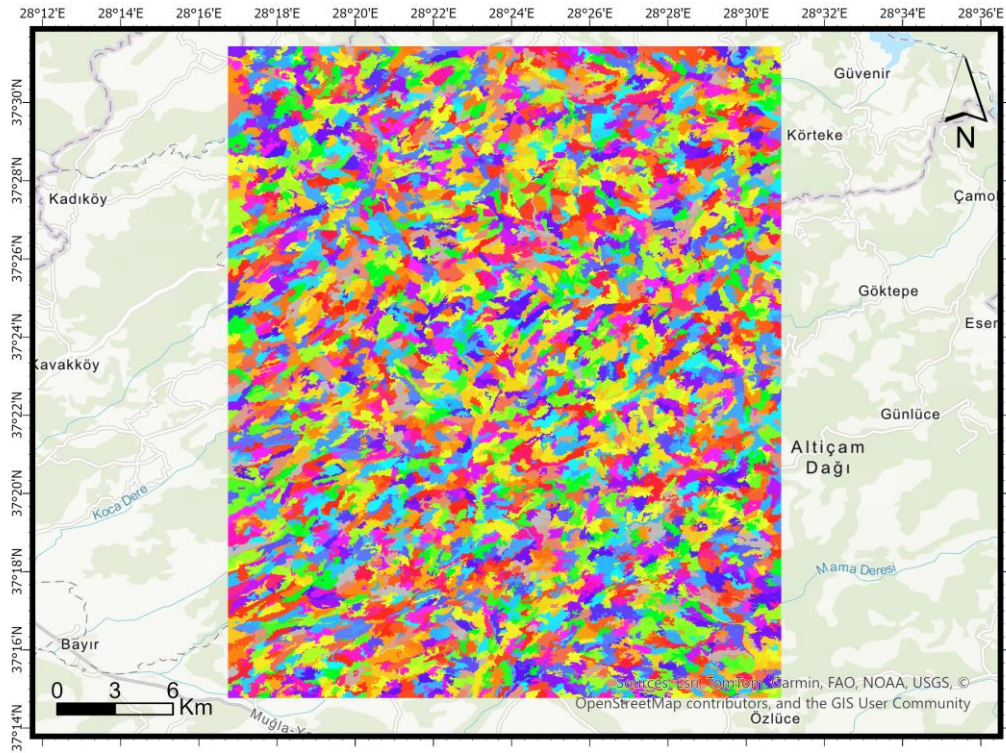


Figure 4.3. The result of SNIC segmentation for study area KV.

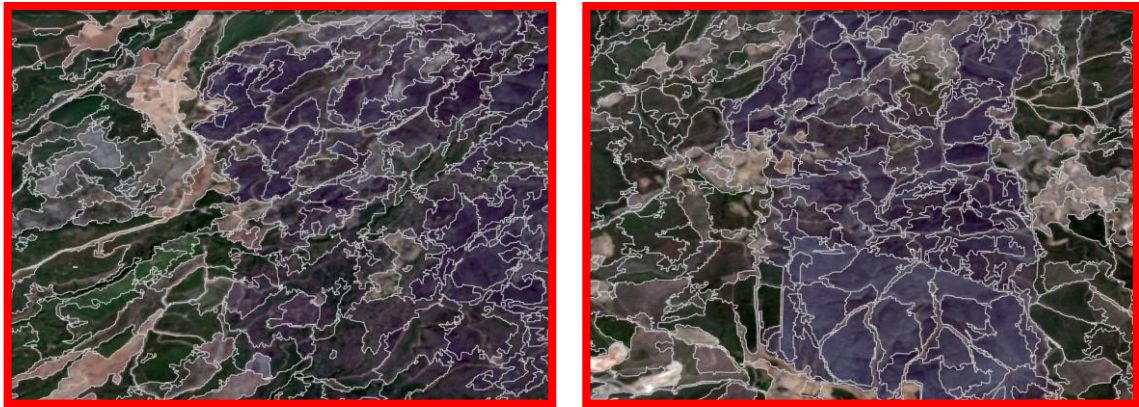
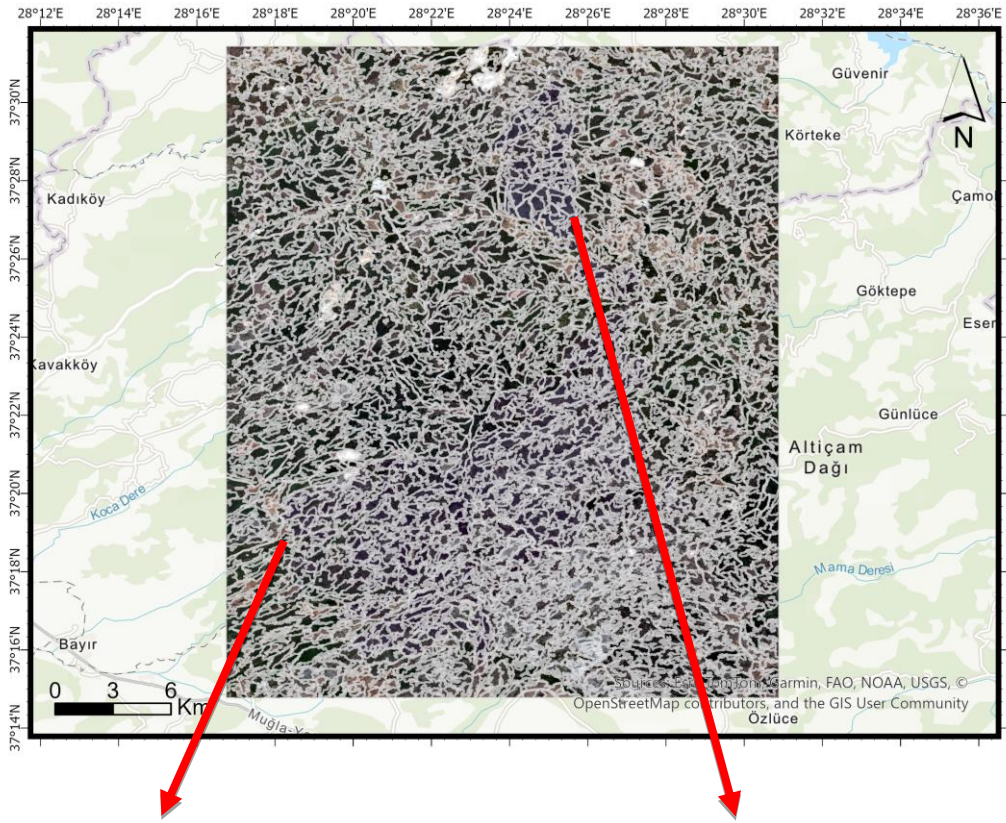


Figure 4.4. The segments in vector form for study area KV (Seed size: 50).

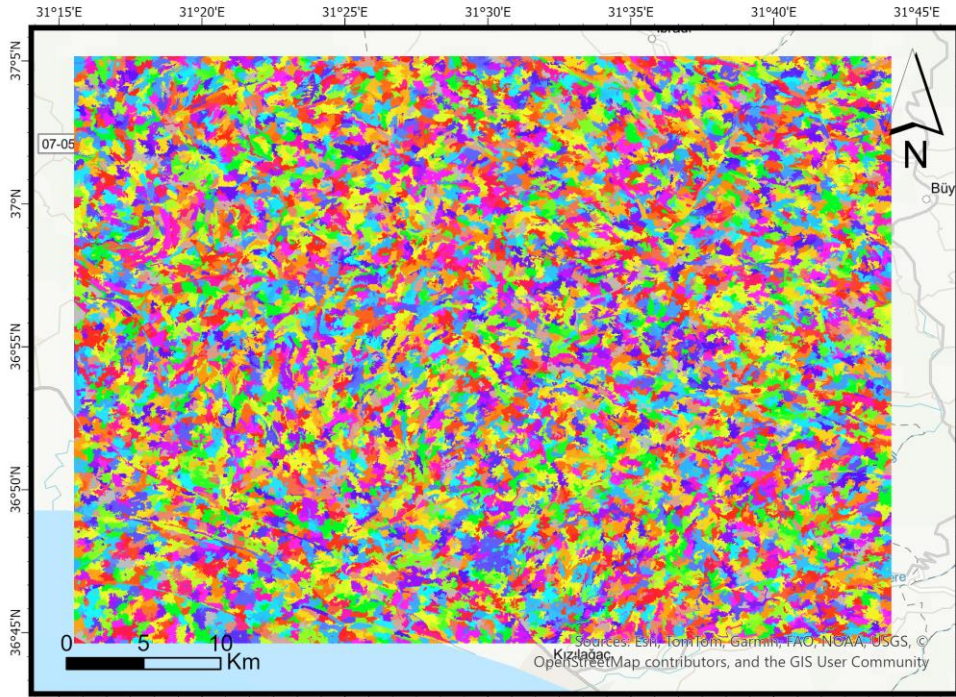


Figure 4.5. The result of SNIC segmentation for study area MG.

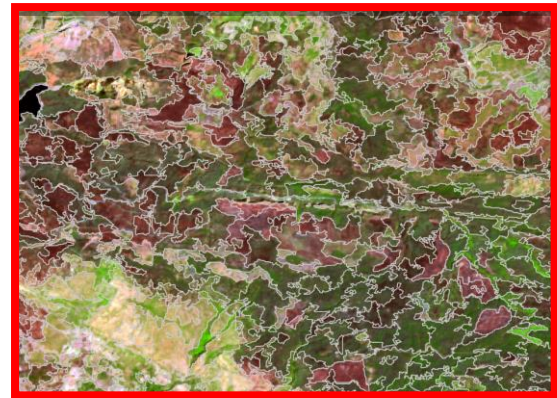
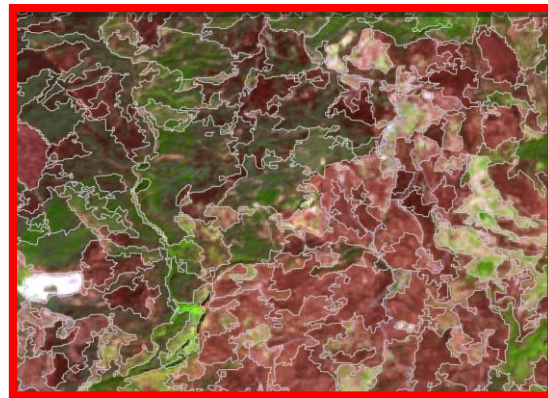
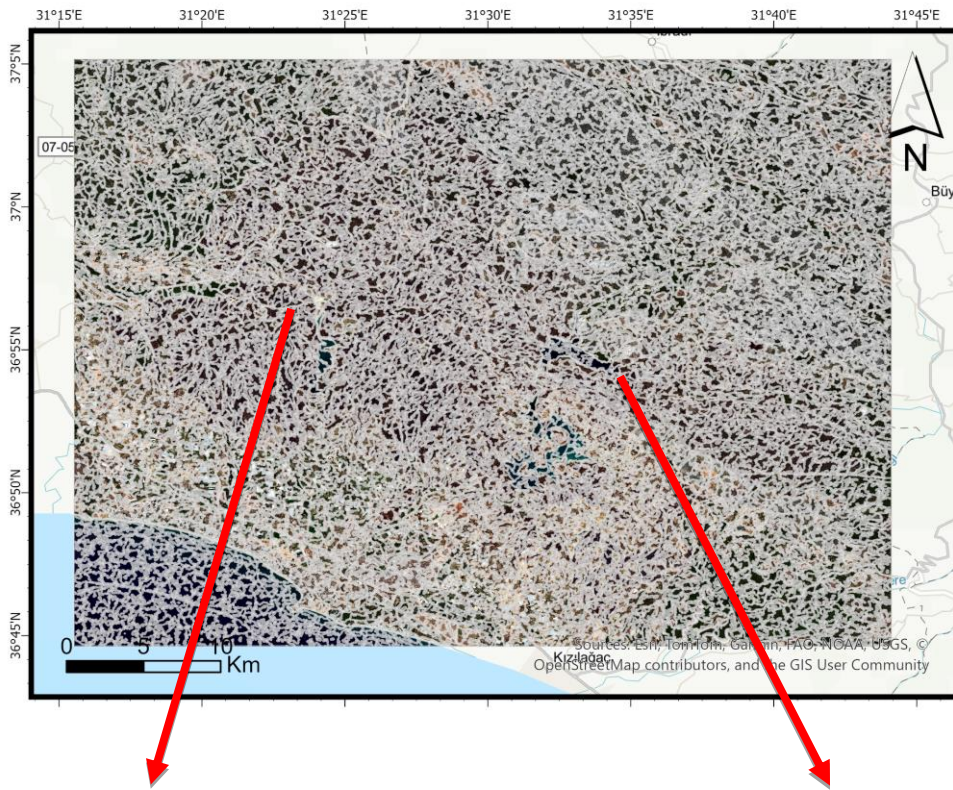


Figure 4.6. The segments in vector form for study area MG (Seed size: 50).

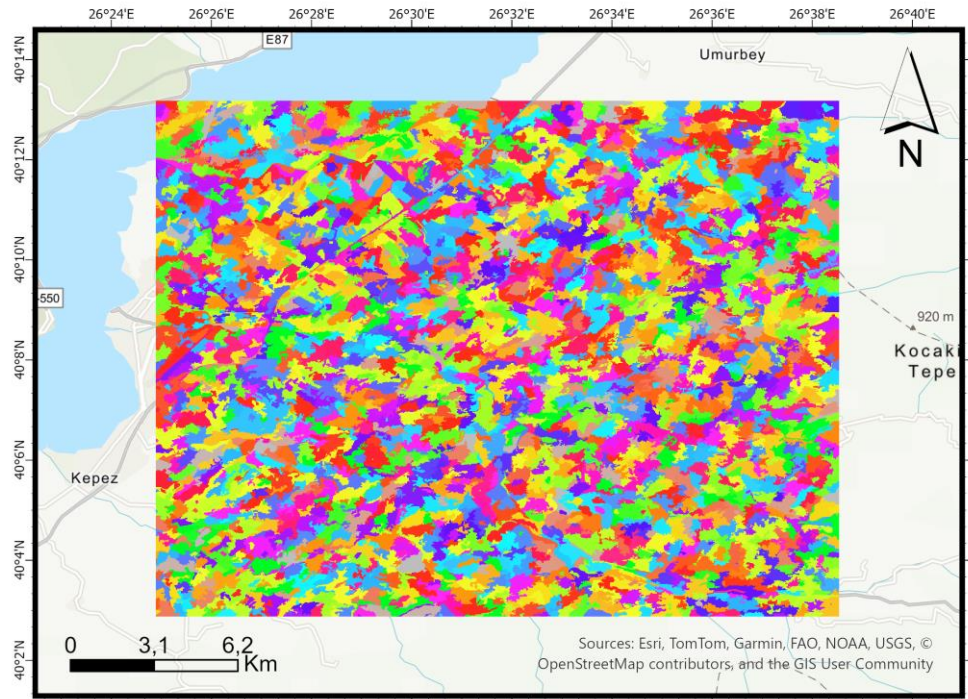


Figure 4.7. The result of SNIC segmentation for study area CK.

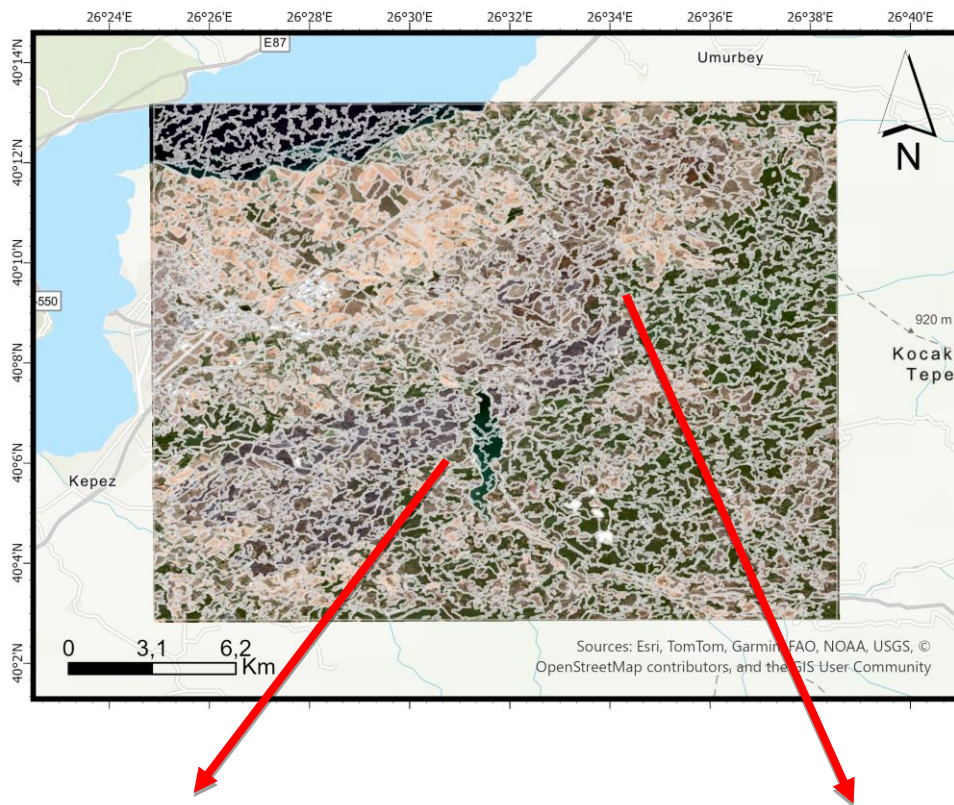
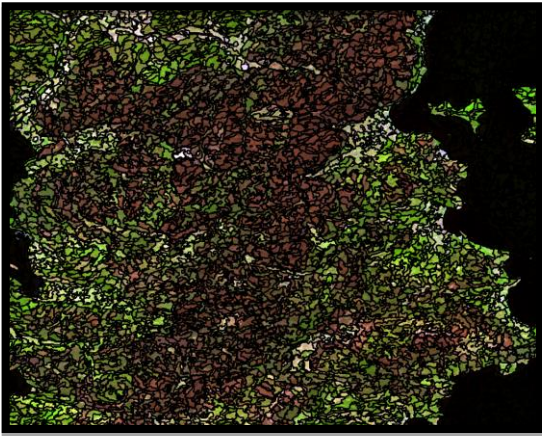
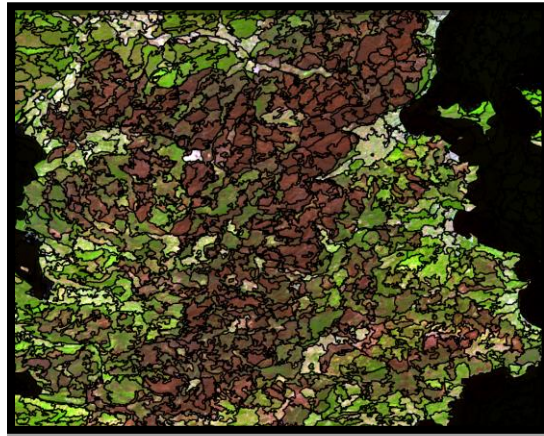


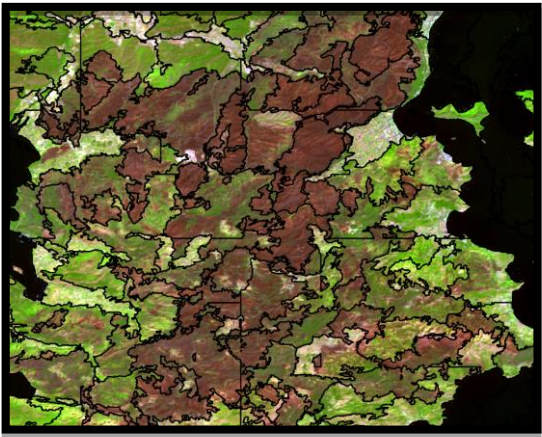
Figure 4.8. The segments in vector form for study area CK (Seed size: 50).



a



b



c



d

Figure 4.9. The result of SNIC segmentation for study area MR. a) seed size: 25, b) seed size: 50, c) seed size: 150, d) seed size: 250

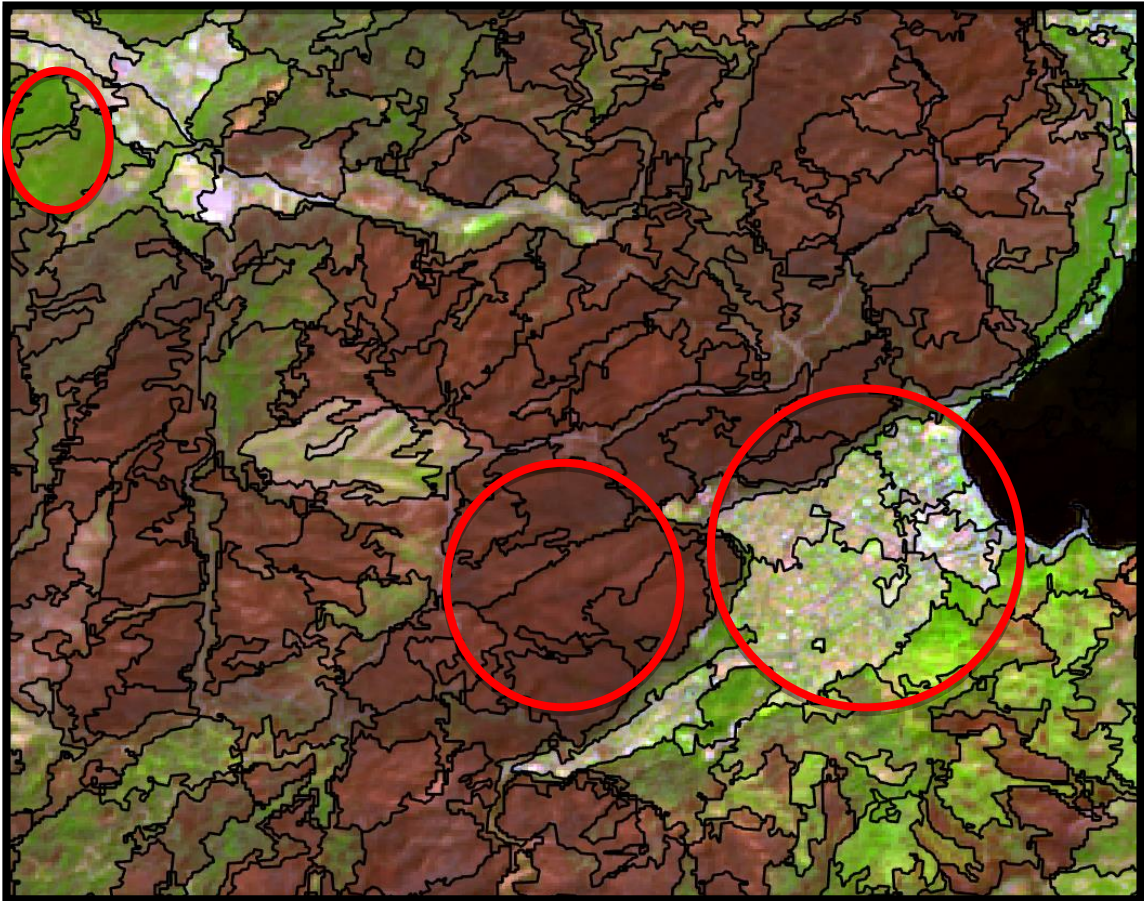


Figure 4.10. Several examples (red circled areas) for illustrating over-segmentation from study area MR (Seed size: 50).

4.2. Burned Area Maps

After the segmentation stage, training data were collected from all study areas. Then, for each study area, the RF algorithm was trained with the training data collected for the study area being considered, and the burned area maps were generated based on the object-based classification logic. Figures 4.11, 4.12, 4.13, and 4.14 respectively show the burned area maps generated for study areas MR, KV, MG, and CK. These maps, produced at 10 m resolution from Sentinel-2 images after the fire, are a valuable resource for studies such as understanding the impact of the fire after the fire and creating rapid action plans. In addition, the possibility of free access to Sentinel-2 images makes these images a valuable resource for the rapid assessment of forest fire effects, as well as developing novel methods and producing accurate burned area maps.

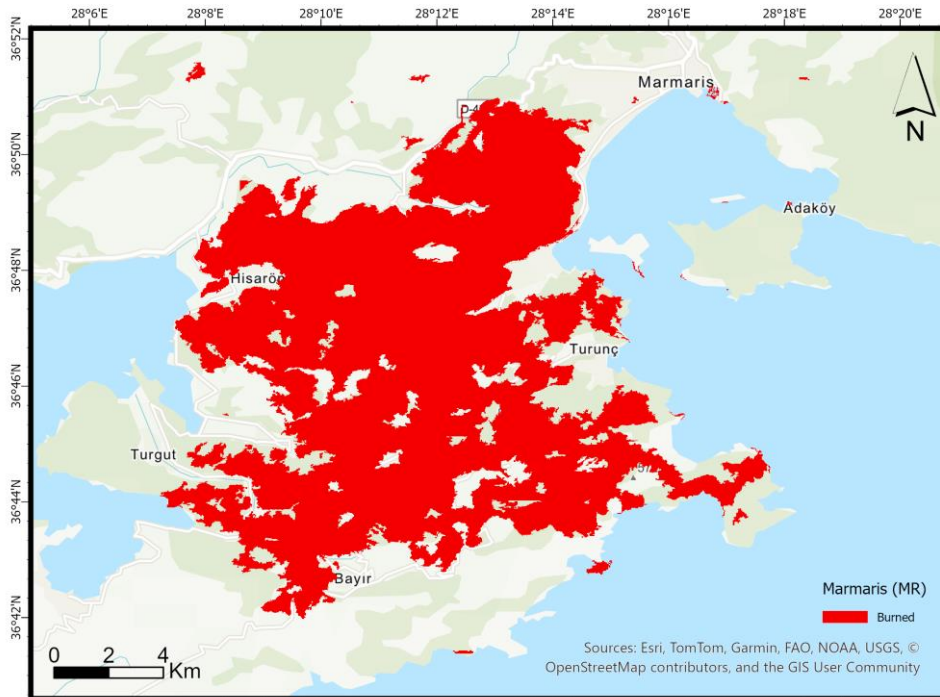


Figure 4.11. Burned-area map of study area MR obtained through object-based RF classification of the post-fire Sentinel-2 image.

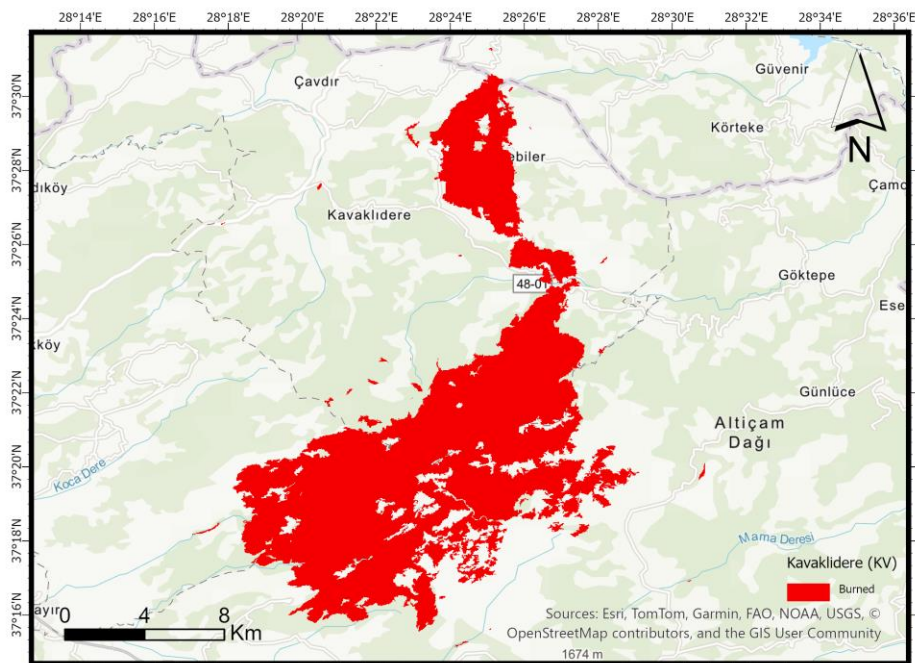


Figure 4.12. Burned-area map of study area KV obtained through object-based RF classification of the post-fire Sentinel-2 image.

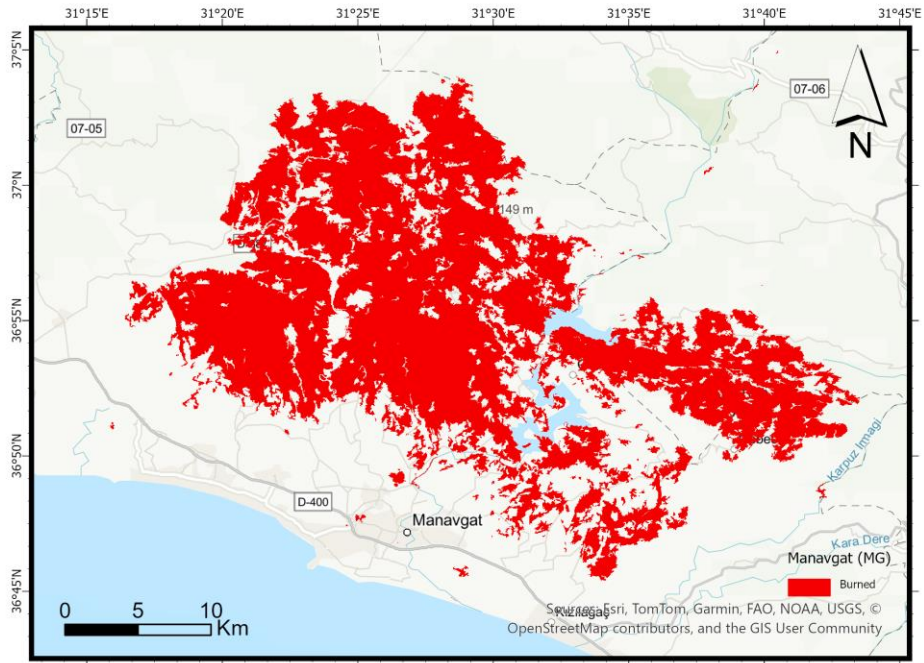


Figure 4.13. Burned-area map of study area MG obtained through object-based RF classification of the post-fire Sentinel-2 image.

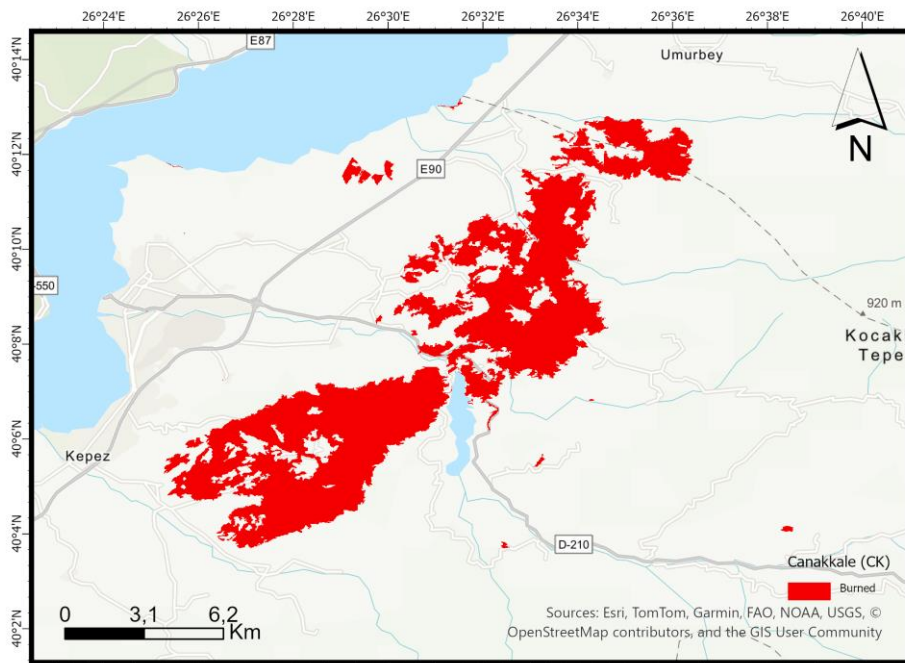


Figure 4.14. Burned-area map of study area CK obtained through object-based RF classification of the post-fire Sentinel-2 image.

4.3. Burned Area Maps Based on Model Transferability

The spatial transferability of the RF model, which was trained based on two study areas (MG and CK), was evaluated on all study areas. To do that object-based classification was applied to all study areas using the model trained based on these two study areas. The difference in the model is that only the data used changed in training the model. All the parameters of the RF classification algorithm and the SNIC segmentation algorithm were kept constant. As described in the chapter 3.4., the algorithm was trained with the training samples collected from the study areas MG and CK, which were selected as the source domain, and then applied to all study areas to extract burned areas through object-based classification. Figures 4.15, 4.16, 4.17, and 4.18 illustrate the burned area maps and the spatial distribution of the burned forest areas extracted by applying transfer learning of the RF algorithm.

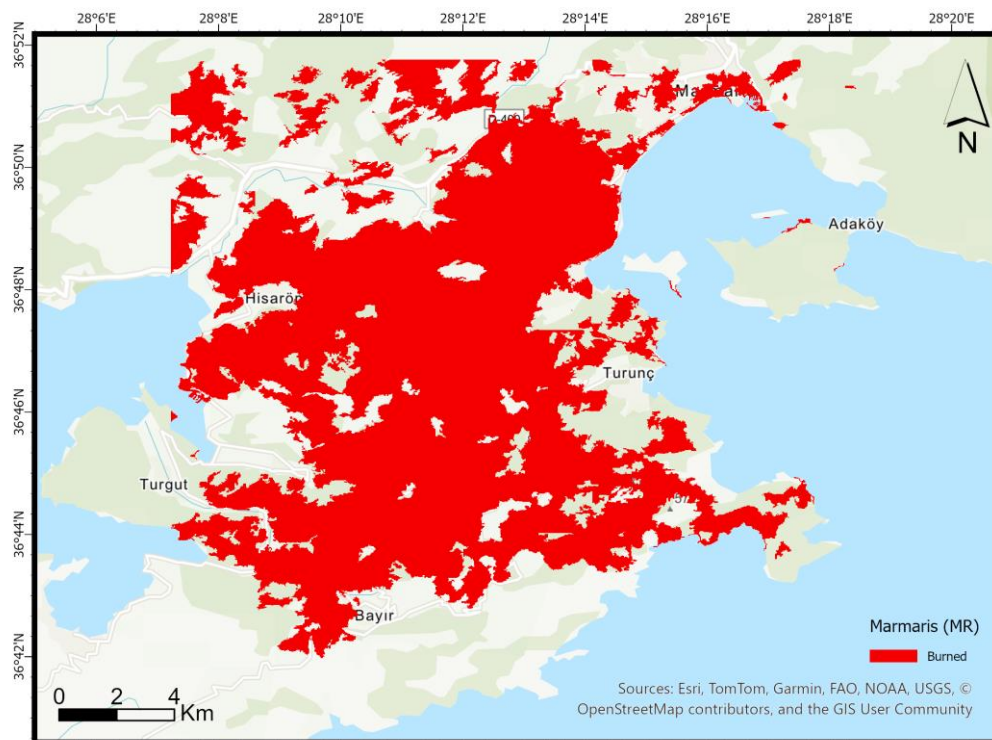


Figure 4.15. Burned-area map of MR obtained through transferability of the RF model.

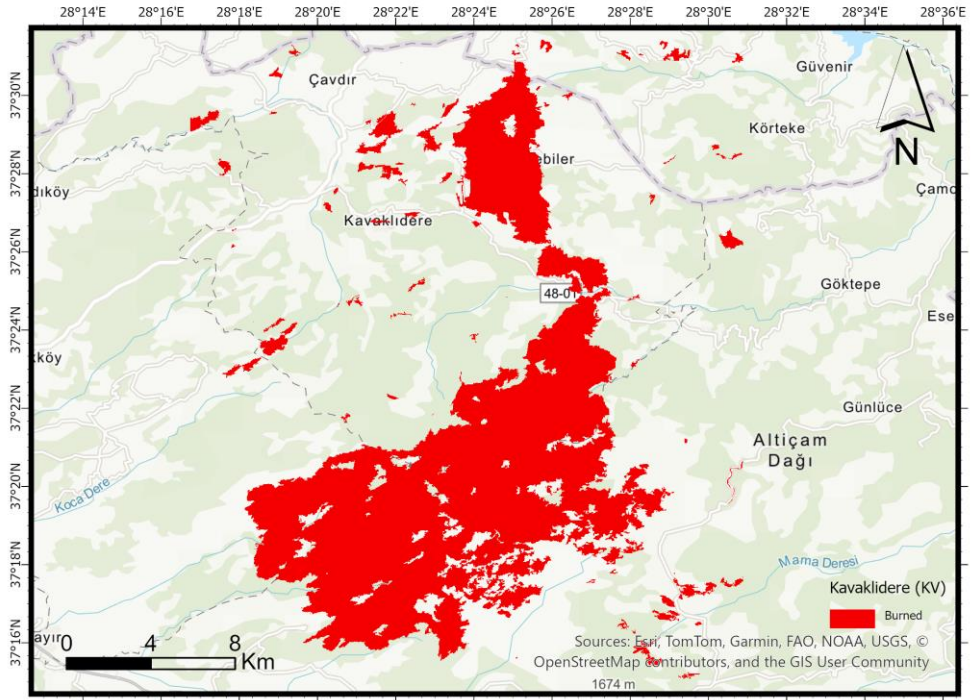


Figure 4.16. Burned-area map of KV obtained through transferability of the RF model.

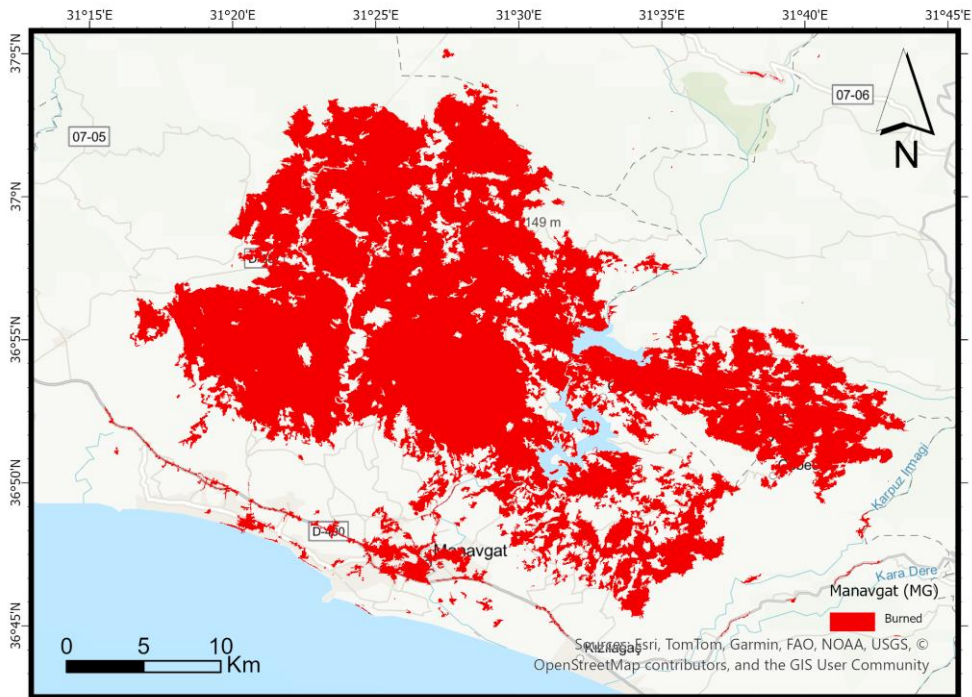


Figure 4.17. Burned-area map of MG obtained through transferability of the RF model.

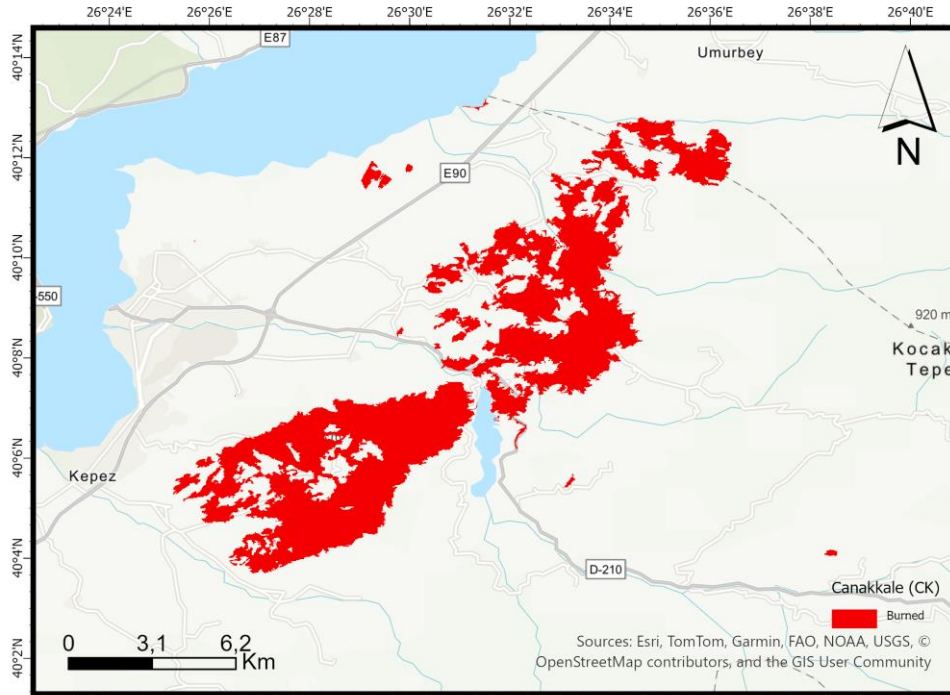


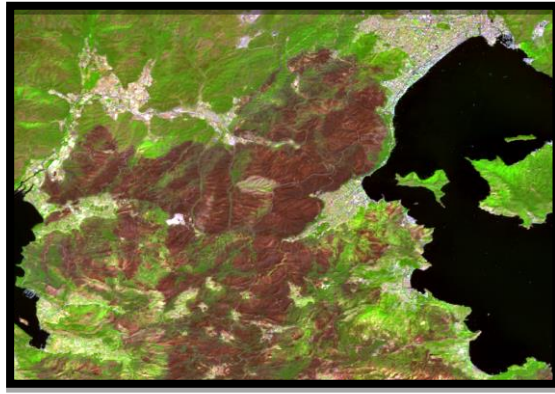
Figure 4.18. Burned-area map of CK obtained through transferability of the RF model.

In order to observe misclassifications occurred in burned area maps based on the RF model transferability, the classification maps and the composite images were visually compared and analyzed. In figure 4.19, several areas selected from study areas MG and MR where transferability did not give correct results are shown. Figures 4.19 a, b and c show a subset of the study area MG where the model transferability gave incorrect results. To remind, MG was one of the source domain study areas. When Figures 4.19 b and c are compared, it is observed that the transferred model provided results with misclassification in shaded areas, some agricultural areas according to the vegetation period, roads and bare soil cover. Figures 4.19 d, e and f show the comparative results for study area MR, which was not the source domain and no training data from this study area was used for training the model. Comparing Figures 4.19 e and f, the predominantly maquis areas described in detail in chapter 2.2.1 are misclassified by the transferred model. The misclassifications given in Figure 4.19 c are among the expected results for the source domains due to the inclusion of training samples from another domain in the model, although one of the given sample study areas is the source domain. Similarly, the misclassifications given in Figure 4.19 f are among the expected

results of applying the model trained with data from other study areas to the MG study area without collecting data specific to the MG study area. Compared to Figure 4.19 e, it is observed that some maquis areas and degraded stand areas are mixed with burned areas. Despite these confusions between the classes, it is considered that the transferability of the RF model provided satisfactory results in the study areas used in this work.



a



d



b



e



c



f

Figure 4.19. (a) For a selected region of MG, false color display of the post-fire Sentinel-2 image. (b) Burned-area map obtained by using RF model. (c) Burned-area map obtained by using RF model transferability. (d) For a selected region of MR, false color display of the post-fire Sentinel-2 image. (e) Burned-area map obtained by using RF model. (f) Burned-area map obtained by using RF model transferability.

4.4. Accuracy Values

Table 4.1 presents the OA and Kappa values of the results of the object-based RF classification and the classification based on RF model transferability. The results were validated based on high-resolution Google Maps and true color and false color Sentinel-2 images. The RF classifier resulted in an OA of over 93% in all study areas. The highest OA among the study areas was obtained for the study area KV. This study area contains both more forest cover and less heterogeneity compared to other areas. High forest land constitutes about 46% of this study area. This means that the structure of the study area is effective on the classification accuracy. The Kappa values computed for all study areas were above 85%. Similar to OA, the highest Kappa value was obtained for the study area KV. When the transferability of the model is assessed, the OA for all study areas were above 85%. On the other hand, the Kappa values were above 72% for all study areas.

The transferability of the RF model appears to be most successful in the study area CK, which provided the highest OA value of 96.8%. This study area was one of the study areas selected as the source domain for testing the RF model transferability. This is associated with the transferability of the model giving the highest accuracy in this study area. However, there was some decrease in the accuracy of the other source domain, the study area MG. The accuracy for the study areas MR and KV that were not selected as source areas decreased.

Figure 4.20 presents the confusion matrices computed for the study areas used in the study. Figure 4.21 shows the UA values and PA values of the classification results. For all study areas, both RF model and RF model transferability produced UA values higher than 77% and PA values higher than 85%. Except for study area CK, in all other study areas the RF model produced higher UA values than the RF model transferability for both classes (burned & unburned). In the case of PA, except for study area MG, in all other study areas the RF model provided higher values than the RF model transferability for the class burned.

Table 4.1. OA and Kappa coefficients resulting from object-based RF classification and RF model transferability for all study areas.

Study Area	RF		RF Transferability	
	OA	Kappa	OA	Kappa
MR	93.5%	85.3%	87.5%	72.8%
KV	97.7%	92.8%	94.8%	84.5%
MG	94.8%	87%	93.6%	84.5%
CK	96.5%	85.9%	96.8%	86.7%

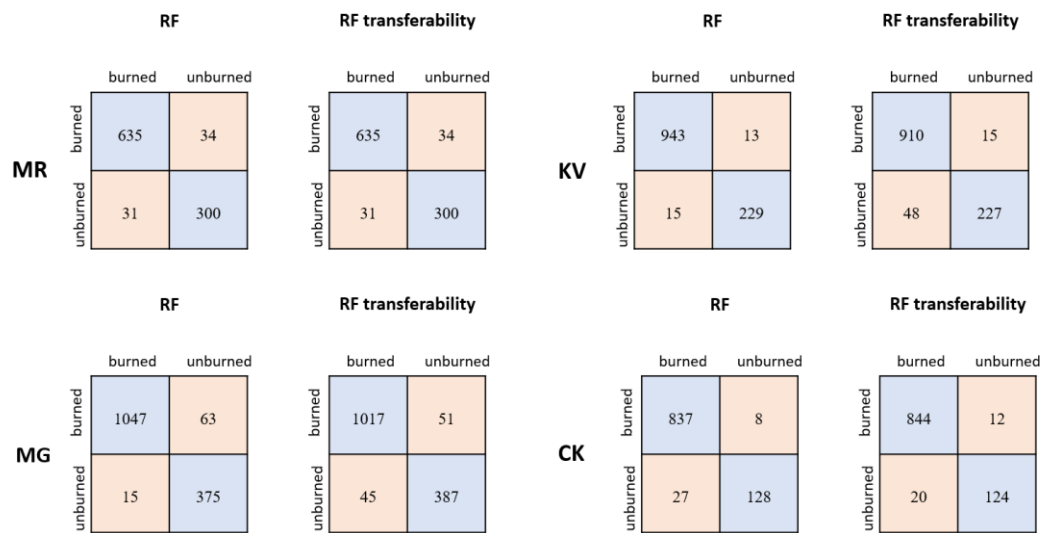


Figure 4.20. For all study areas, the confusion matrices computed for the RF model and RF model transferability.

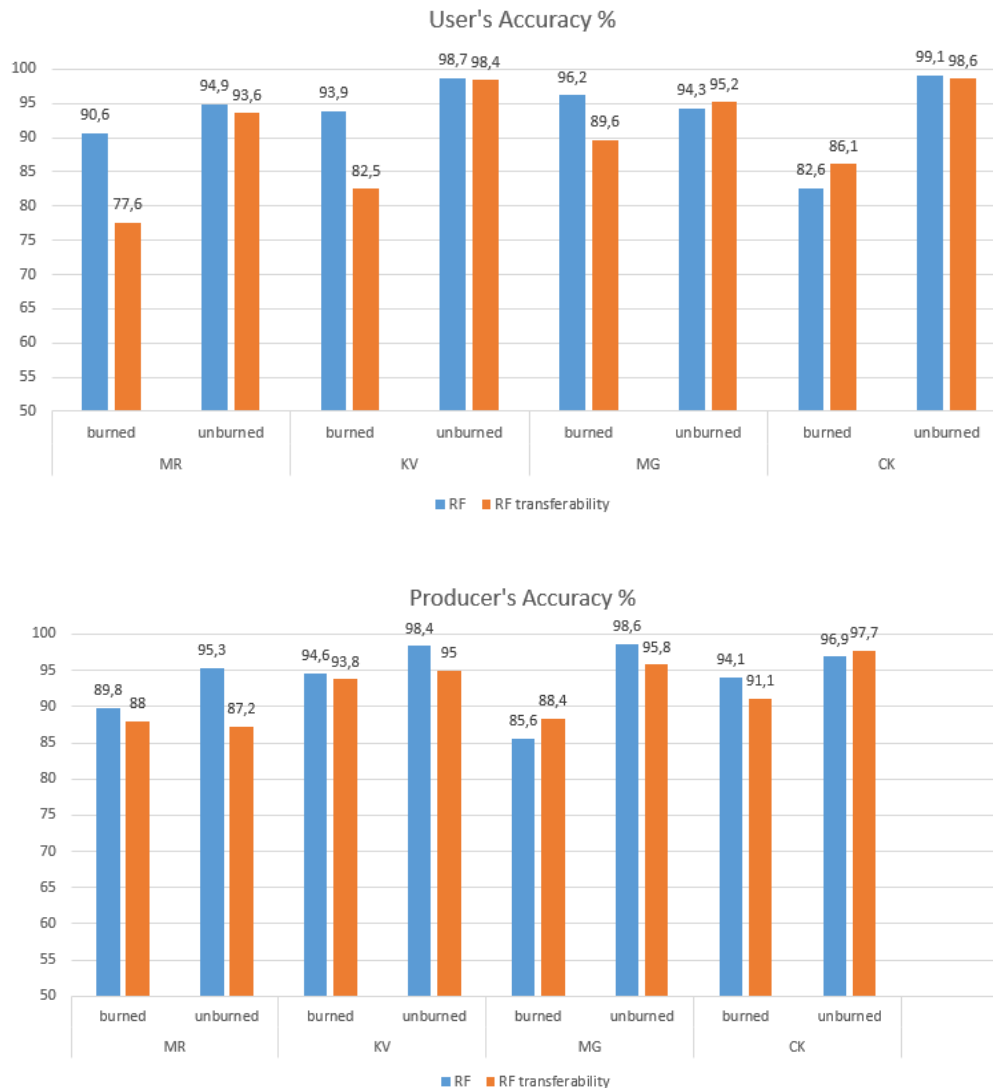


Figure 4.21. PA and UA values computed for the RF model and RF transferability

As it was mentioned earlier (Chapter 3.4), the collected samples were randomly divided into 70 per cent as training data and 30 per cent as validation data. With the data allocated for validation, an accuracy score was calculated to evaluate how the RF algorithm performs with data it has not seen before. The RF model trained based on the data sets of study areas MR, KV, MG and CK provided the accuracy values of 92.31%, 97.73%, 94.23% and 95% respectively on test data. For the evaluation of the transferability of the RF model, the trained model provided an accuracy score of 93.6% on the test data of the source domains MG and CK.

4.5. Inter-comparison with ancillary data

The burned-area maps generated using the object-based RF classification approach and the RF model transferability were compared with the C3S - C3SBA10, MODIS - MCD64A1 and EFFIS as global burned area datasets and General Directorate of Forestry data as national burned area data on hectare basis (Table 4.2). The purpose of this comparison was not to validate the obtained results. It was to reflect the differences and uncertainties of the burned area information between different global and national data sets.

As shown in Figure 4.22, the burned scar shape and spatial information obtained by the applied object-based RF image classification method on the post-fire Sentinel-2 images are in close agreement with the global data sets. Differences in the spatial, spectral and temporal resolution of the compared global burned area products, and differences in the data and methods used for burned area information are among the reasons for the difference in burned area information.

The difference in burned area information between different sensors can also be related to the heterogeneity of the burned areas. In those study sites with heterogeneous land cover types, unburned areas can be included in the information from coarse resolution sensors, leading to a higher burned area information [67]. In addition, the EFFIS maps show fires that occurred in the forested and semi-natural areas and does not include agricultural areas [68]. In the study of [68] it was shown that when the comparison between Modis and EFFIS data is reduced to only forest and semi-natural areas, the differences between the burned areas reduce, but since the difference persists, they emphasized that the differences between the two products should be associated with other factors. The authors also emphasized that since EFFIS data is in vector format and is a digitization product, it also contains generalization error. In the study conducted by [66], EFFIS data were used as ground truth data to evaluate the accuracy of the MODIS MCD64A1 dataset over the fires that occurred in Türkiye between 2015-2020 and the accuracy of the MCD64A1 data was evaluated. A precision of 93.81% and an F1 score of 79.38% were reported for the MCD64A1 data.

Table 4.2. Comparison of the burned areas detected in this study with the burned-areas provided by the data sets MCD64A1, C3SBA10, EFFIS, and GDF. *The C3SBA10 dataset did not contain burned area information for study area CK . The values are in hectares.

	Study Areas			
	MR	KV	MG	CK
RF	10724,16	13083,46	41960,69	5729,73
RF Transferability	12078,63	14437,54	47799,99	5203,40
MCD64A1	12478,53	15175,97	57799,43	6911,64
C3SBA10	7820,29	13112,70	33367,12	-*
EFFIS	11548,00	15322,00	54769,00	7031,00
GDF	9051,60	16331,00	48412,00	3869,75

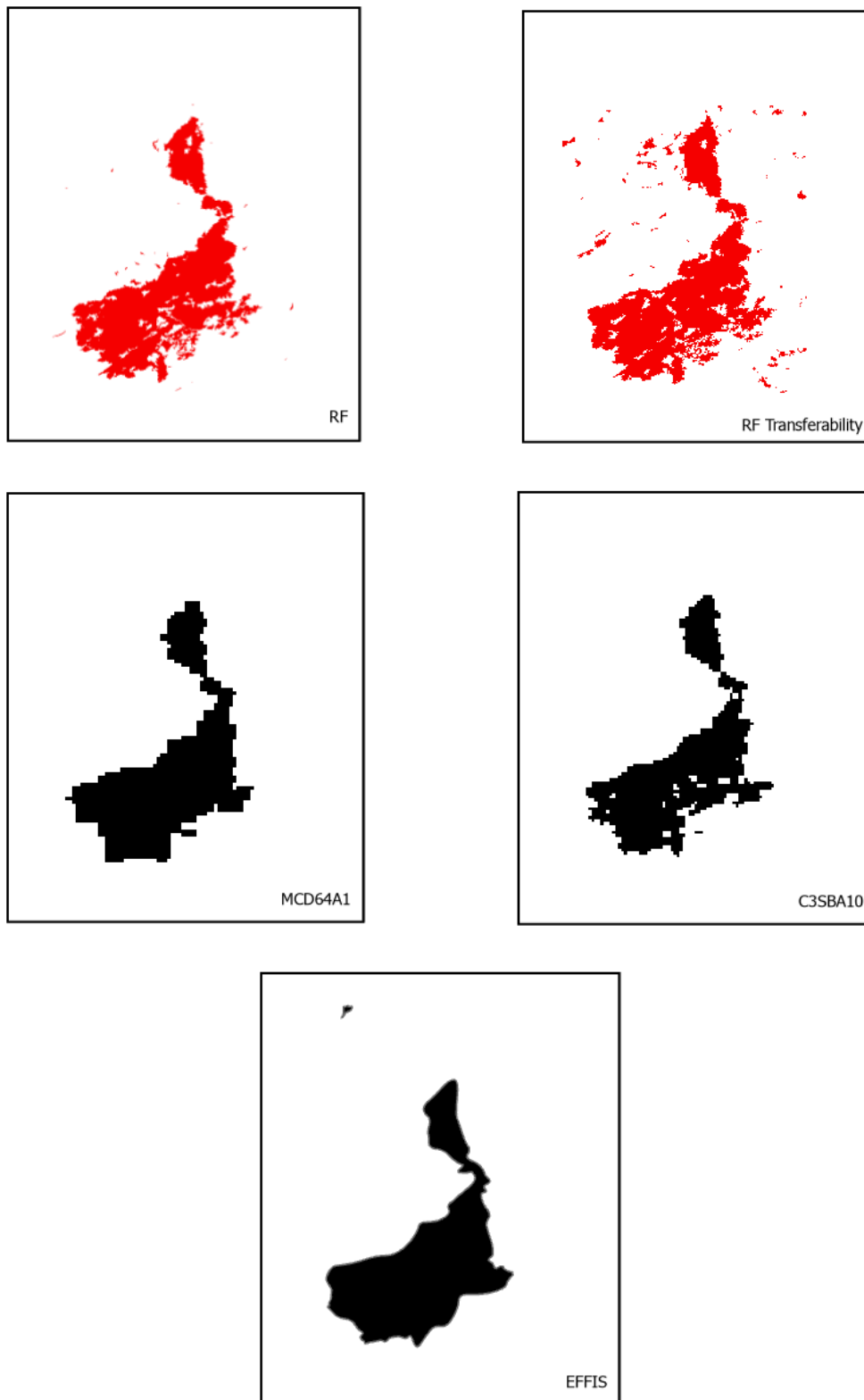


Figure 4.22. For study area KV, comparison of the detected burned areas (shown in red color) with the burned areas provided by the data sets MCD64A1, C3SBA10, and EFFIS. *GDF data was not included as it is not in spatial form.

5. CONCLUSIONS

Detection of burned forest areas from satellite imagery has been investigated in the previous studies using the ML algorithms and object-based classification method, however studies based on post-fire Sentinel-2 imagery using the object-based method on cloud-based platform remain limited. In this study, SNIC segmentation and RF machine learning algorithm were integrated on GEE platform, which is a free geospatial processing and analysis platform, and burned areas in four different study sites were successfully extracted from post-fire Sentinel-2 images through object-based classification logic. After pre-processing operations (downscaling, clipping, mosaicking etc.) the Sentinel-2 images were made ready to be used for achieving the segmentation stage. After performing image segmentation, object-based RF classification was carried out on the segmented image. Furthermore, the transferability of the RF model was evaluated on the study areas.

The principal conclusion to be drawn from this study is that the proposed object-based RF classification approach applied in four different study areas provided quite satisfactory results. When the transferability of the model is evaluated, the results are still satisfactory, although there is a decrease in the OA.

The fundamental conclusions obtained in this study can be summarized as follows:

- The results show that the object-based RF model can be effectively used for the detection and mapping of burned forest areas with an OA of over 93%.
- The results with the OA of over 85% obtained through transferability of the RF model demonstrate that the utilized object-based RF model has a high potential to be implemented in different parts of Türkiye, where the land cover types are Mediterranean forests, woodlands, and shrublands.
- The results show that the post-fire uni-temporal approach can be successfully applied with the post-fire Sentinel-2 imagery to extract and map burned forest areas. The uni-temporal approach on post-fire image facilitated the application speed, reduced data and analysis requirements, and highlighted the usefulness of the uni-temporal approach in the detection of burned forest areas.

- Based on the visual interpretation of the results it can be stated that the selection of the SNIC segmentation parameter values have a significant effect on the segmentation results of the 10 m Sentinel-2 imagery and effect the results of object-based classification. Different segmentation parameters affect the size and number of the image objects, which can directly affect the classification results. The seed size parameter, which defines the super pixel seed position range in pixels, was found to be highly effective on the segmentation results. Therefore, it is important to test and evaluate the seed size parameter and other segmentation parameters to achieve the best segmentation results, as failure to select the appropriate parameter may lead to over- or under-segmentation and directly affect the classification results.
- Certain level of inconsistencies exist between the burned area maps generated by the used approach and the global burned area data sets (C3SBA10, MCD64A1, EFFIS) and GDF data, demonstrating the amount of burned area. . The fact that global burned area data are inconsistent even among themselves and present different amounts of burned area reveals the importance of accurate, precise and consistent information in burned area data.
- As a result of the tested SNIC parameters, smaller sized segments resulted in a higher number of segments, and as the study area increased, the number of segments to be classified increased and the processing time increased. This may lead to long and heavy analyses or errors due to the computational and memory limitations of GEE [37, 99].
- The use of the cloud-based and free GEE platform for the entire study allows users to quickly analyze high-resolution satellite imagery for assessing wildfire damage, developing response plans and other relevant analyses on a single platform, independent of computer processing power.

Overall, this study demonstrates that object-based ML classification of the 10-metre resolution post-fire uni-temporal Sentinel-2 data can be effectively used to detect burned forest areas using the cloud-based GEE platform. This study also shows that the trained model can be applied for rapid assessment of potential fires in Mediterranean forests, woodlands and shrublands biome specific areas in Türkiye. Furthermore, this

study highlights that the GEE platform has the potential to be a powerful and preferred tool for disaster management, especially for forest fires.

6. REFERENCES

- [1] E.G. Brockerhoff, L. Barbaro, B. Castagneyrol, D.I. Forrester, B. Gardiner, J.R. González-Olabarria, P.O.B. Lyver, N. Meurisse, A. Oxbrough, H. Taki, Forest biodiversity, ecosystem functioning and the provision of ecosystem services, Springer, **2017**, pp. 3005-3035.
- [2] FAO, Global Forest Resources Assessment 2020: Main report. Rome., (**2020**).
- [3] J.P. Kimmins, Forest ecology, Fishes and forestry: Worldwide watershed interactions and management, (**2004**) 17-43.
- [4] B. Langmann, B. Duncan, C. Textor, J. Trentmann, G.R. Van Der Werf, Vegetation fire emissions and their impact on air pollution and climate, Atmospheric environment, 43 (**2009**) 107-116.
- [5] GFW, Global Forest Watch, <https://www.globalforestwatch.org/>, (Access date : 28 May **2024**).
- [6] OGM, Orman Genel Mudurlugu, <https://www.ogm.gov.tr/tr/e-kutuphane/resmi-istatistikler>, (Access date : 28 May **2024**).
- [7] C. Maffei, M. Menenti, Predicting forest fires burned area and rate of spread from pre-fire multispectral satellite measurements, ISPRS Journal of Photogrammetry and Remote Sensing, 158 (**2019**) 263-278.
- [8] R. Çömert, D.K. Matci, U. Avdan, Object based burned area mapping with random forest algorithm, International Journal of Engineering and Geosciences, 4 (**2019**) 78-87.
- [9] C. Amos, G.P. Petropoulos, K.P. Ferentinos, Determining the use of Sentinel-2A MSI for wildfire burning & severity detection, International journal of remote sensing, 40 (**2019**) 905-930.
- [10] E. Çolak, F. Sunar, Evaluation of forest fire risk in the Mediterranean Turkish forests: A case study of Menderes region, Izmir, International journal of disaster risk reduction, 45 (**2020**) 101479.

- [11] D.W. Huffman, J.P. Roccaforte, J.D. Springer, J.E. Crouse, Restoration applications of resource objective wildfires in western US forests: a status of knowledge review, *Fire Ecology*, 16 (2020) 1-13.
- [12] S. Bar, B.R. Parida, A.C. Pandey, Landsat-8 and Sentinel-2 based Forest fire burn area mapping using machine learning algorithms on GEE cloud platform over Uttarakhand, Western Himalaya, *Remote Sensing Applications: Society and Environment*, 18 (2020) 100324.
- [13] N. Harris, R. Petersen, C. Davis, O. Payne, INSIDER: Global Forest Watch and the Forest Resources Assessment, Explained in 5 Graphics, (2016).
- [14] E. Chuvieco, F. Mouillot, G.R. Van der Werf, J. San Miguel, M. Tanase, N. Koutsias, M. García, M. Yebra, M. Padilla, I. Gitas, Historical background and current developments for mapping burned area from satellite Earth observation, *Remote Sens Environ*, 225 (2019) 45-64.
- [15] K. Lalitha, G. Veerapandu, Forest fire detection using satellite images, *Proceedings of Second International Conference in Mechanical and Energy Technology: ICMET 2021, India, Springer, 2022*, pp. 277-284.
- [16] P. Palaiologou, K. Kalabokidis, P. Kyriakidis, Forest mapping by geoinformatics for landscape fire behaviour modelling in coastal forests, Greece, *International journal of remote sensing*, 34 (2013) 4466-4490.
- [17] P. Roy, Forest fire and degradation assessment using satellite remote sensing and geographic information system, *Satellite Remote sensing and GIS applications in agricultural meteorology*, (2003) 361-400.
- [18] D.B. Wright, T. Yotsumata, N. El-Sheimy, C. Liu, Real time identification and location of forest fire hotspots from geo-referenced thermal images, *International Archives of Photogrammetry Remote Sensing and Spatial Information Sciences*, 35 (2004) 13-18.
- [19] T. Holloway, D. Miller, S. Anenberg, M. Diao, B. Duncan, A.M. Fiore, D.K. Henze, J. Hess, P.L. Kinney, Y. Liu, Satellite monitoring for air quality and health, *Annual review of biomedical data science*, 4 (2021) 417-447.

- [20] R.K. Jaiswal, S. Mukherjee, K.D. Raju, R. Saxena, Forest fire risk zone mapping from satellite imagery and GIS, *International journal of applied earth observation and geoinformation*, 4 (2002) 1-10.
- [21] J.-H. Zhang, F.-M. Yao, C. Liu, L.-M. Yang, V.K. Boken, Detection, emission estimation and risk prediction of forest fires in China using satellite sensors and simulation models in the past three decades—An overview, *International journal of environmental research and public health*, 8 (2011) 3156-3178.
- [22] D.O.S. Hsbalkhalig, Efficiency Evaluation of MODIS Data Products in Monitoring and Mapping the Wild land Fire, *Sudan University of Science and Technology*, 2019.
- [23] İ. Taşcı, Z.Y. Avdan, U. Avdan, R. Çömert, Orta çözünürlüklü uydu görüntülerinden değişim saptama ile yanmış orman alanlarının haritalanması, VII. Uzaktan Algılama-CBS Sempozyumu (UZAL-CBS 2018)Eskişehir, 2018.
- [24] A. Banskota, N. Kayastha, M.J. Falkowski, M.A. Wulder, R.E. Froese, J.C. White, Forest monitoring using Landsat time series data: A review, *Canadian Journal of Remote Sensing*, 40 (2014) 362-384.
- [25] C. Kalogeropoulos, G. Amatulli, P. Kempeneers, F. Sedano, J. San Miguel-Ayanz, A. Camia, Mapping burned areas and burn severity patterns across the Mediterranean region, *EGU General Assembly Conference Abstracts*, 2010, pp. 12573.
- [26] A.d.P. Pacheco, J.A.d.S. Junior, A.M. Ruiz-Armenteros, R.F.F. Henriques, Assessment of k-nearest neighbor and random forest classifiers for mapping forest fire areas in central portugal using landsat-8, sentinel-2, and terra imagery, *Remote Sensing*, 13 (2021) 1345.
- [27] H. Achour, A. Toujani, H. Trabelsi, W. Jaouadi, Evaluation and comparison of Sentinel-2 MSI, Landsat 8 OLI, and EFFIS data for forest fires mapping. Illustrations from the summer 2017 fires in Tunisia, *Geocarto International*, 37 (2022) 7021-7040.
- [28] P. Konkathi, A. Shetty, Inter comparison of post-fire burn severity indices of Landsat-8 and Sentinel-2 imagery using Google Earth Engine, *Earth Science Informatics*, 14 (2021) 645-653.

- [29] E. Alcaras, D. Costantino, F. Guastaferro, C. Parente, M. Pepe, Normalized Burn Ratio Plus (NBR+): a new index for Sentinel-2 imagery, *Remote Sensing*, 14 (2022) 1727.
- [30] S. Arellano-Pérez, A.D. Ruiz-González, J.G. Álvarez-González, J.A. Vega-Hidalgo, R. Díaz-Varela, C. Alonso-Rego, Mapping fire severity levels of burned areas in Galicia (NW Spain) by Landsat images and the dNBR index: Preliminary results about the influence of topographical, meteorological and fuel factors on the highest severity level, *Advances in Forest Fire Research*, (2018) 1053-1060.
- [31] Y.E. Shimabukuro, A.C. Dutra, E. Arai, V. Duarte, H.L.G. Cassol, G. Pereira, F.d.S. Cardozo, Mapping burned areas of Mato Grosso state Brazilian Amazon using multisensor datasets, *Remote Sensing*, 12 (2020) 3827.
- [32] J. Florath, S. Keller, Supervised machine learning approaches on multispectral remote sensing data for a combined detection of fire and burned area, *Remote sensing*, 14 (2022) 657.
- [33] N. Georgopoulos, D. Stavrakoudis, I.Z. Gitas, Object-Based Burned Area Mapping Using Sentinel-2 Imagery and Supervised Learning Guided by Empirical Rules, *IGARSS 2019-2019 IEEE International Geoscience and Remote Sensing Symposium*, IEEE, 2019, pp. 9980-9983.
- [34] J. Liu, D. Freudenberger, S. Lim, Mapping burned areas and land-uses in Kangaroo Island using an object-based image classification framework and Landsat 8 Imagery from Google Earth Engine, *Geomatics, Natural Hazards and Risk*, 13 (2022) 1867-1897.
- [35] A. Polychronaki, I.Z. Gitas, Burned area mapping in Greece using SPOT-4 HRVIR images and object-based image analysis, *Remote Sensing*, 4 (2012) 424-438.
- [36] A. Polychronaki, I.Z. Gitas, The development of an operational procedure for burned-area mapping using object-based classification and ASTER imagery, *International Journal of Remote Sensing*, 31 (2010) 1113-1120.
- [37] A.S. Kulinan, Y. Cho, M. Park, S. Park, Rapid wildfire damage estimation using integrated object-based classification with auto-generated training samples from Sentinel-2 imagery on Google Earth Engine, *International Journal of Applied Earth Observation and Geoinformation*, 126 (2024) 103628.

- [38] L. Ma, M. Li, X. Ma, L. Cheng, P. Du, Y. Liu, A review of supervised object-based land-cover image classification, *ISPRS Journal of Photogrammetry and Remote Sensing*, 130 (2017) 277-293.
- [39] K. Lee, B. Kim, S. Park, Evaluating the potential of burn severity mapping and transferability of Copernicus EMS data using Sentinel-2 imagery and machine learning approaches, *GIScience & Remote Sensing*, 60 (2023) 2192157.
- [40] B. Praveen, S. Mustak, P. Sharma, Assessing the transferability of machine learning algorithms using cloud computing and earth observation datasets for agricultural land use/cover mapping, *The International Archives of the Photogrammetry, Remote Sensing and Spatial Information Sciences*, 42 (2019) 585-592.
- [41] A. Orynbaikyzy, U. Gessner, C. Conrad, Spatial transferability of random forest models for crop type classification using Sentinel-1 and Sentinel-2, *Remote Sensing*, 14 (2022) 1493.
- [42] G.H. Mitri, I.Z. Gitas, A semi-automated object-oriented model for burned area mapping in the Mediterranean region using Landsat-TM imagery, *International Journal of Wildland Fire*, 13 (2004) 367-376.
- [43] N.O. Soverel, N.C. Coops, D.D. Perrakis, L.D. Daniels, S.E. Gergel, The transferability of a dNBR-derived model to predict burn severity across 10 wildland fires in western Canada, *International Journal of Wildland Fire*, 20 (2011) 518-531.
- [44] A. Tassi, D. Gigante, G. Modica, L. Di Martino, M. Vizzari, Pixel-vs. Object-based landsat 8 data classification in google earth engine using random forest: The case study of maiella national park, *Remote sensing*, 13 (2021) 2299.
- [45] N. Gorelick, M. Hancher, M. Dixon, S. Ilyushchenko, D. Thau, R. Moore, Google Earth Engine: Planetary-scale geospatial analysis for everyone, *Remote Sens Environ*, 202 (2017) 18-27.
- [46] İ.H. Saylan, R. Çömert, Sentinel-2A ürünlerinin yanmış orman alanlarının haritalanmasındaki başarımın araştırılması, *Türkiye Uzaktan Algılama Dergisi*, 1 (2019) 8-15.

- [47] P. Barmpoutis, P. Papaioannou, K. Dimitropoulos, N. Grammalidis, A review on early forest fire detection systems using optical remote sensing, *Sensors*, 20 (2020) 6442.
- [48] Y. Gao, M. Skutsch, J. Paneque-Gálvez, A. Ghilardi, Remote sensing of forest degradation: a review, *Environmental Research Letters*, 15 (2020) 103001.
- [49] M.G. Gale, G.J. Cary, A.I. Van Dijk, M. Yebra, Forest fire fuel through the lens of remote sensing: Review of approaches, challenges and future directions in the remote sensing of biotic determinants of fire behaviour, *Remote Sens Environ*, 255 (2021) 112282.
- [50] M. Mohajane, R. Costache, F. Karimi, Q.B. Pham, A. Essahlaoui, H. Nguyen, G. Laneve, F. Oudija, Application of remote sensing and machine learning algorithms for forest fire mapping in a Mediterranean area, *Ecological Indicators*, 129 (2021) 107869.
- [51] E. Sertel, U. Alganci, Comparison of pixel and object-based classification for burned area mapping using SPOT-6 images, *Geomatics, Natural Hazards and Risk*, 7 (2016) 1198-1206.
- [52] I. Kotaridis, M. Lazaridou, Integrating image segmentation in the delineation of burned areas on Sentinel-2 and Landsat 8 data, *Remote Sensing Applications: Society and Environment*, 30 (2023) 100944.
- [53] D. Stavrakoudis, I.Z. Gitas, Object-Based Burned Area Mapping with Extreme Gradient Boosting Using Sentinel-2 Imagery, *Journal of Geographic Information System*, 15 (2023) 53-72.
- [54] P. Liu, Y. Liu, X. Guo, W. Zhao, H. Wu, W. Xu, Burned area detection and mapping using time series Sentinel-2 multispectral images, *Remote Sens Environ*, 296 (2023) 113753.
- [55] E. Roteta, A. Bastarrika, M. Padilla, T. Storm, E. Chuvieco, Development of a Sentinel-2 burned area algorithm: Generation of a small fire database for sub-Saharan Africa, *Remote Sens Environ*, 222 (2019) 1-17.
- [56] E. Bilgiç, G.T. Tuygun, O. Gündüz, Development of an emission estimation method with satellite observations for significant forest fires and comparison with

global fire emission inventories: Application to catastrophic fires of summer 2021 over the Eastern Mediterranean, *Atmospheric Environment*, 308 (2023) 119871.

[57] EFFIS, European Forest Fire Information System, <https://forest-fire.emergency.copernicus.eu/>, (Access date : 28 May 2024).

[58] Copernicus, Copernicus Sentinel-2 MSI, <https://www.copernicus.eu/en>, (Access date : 28 May 2024).

[59] M.L. García, V. Caselles, Mapping burns and natural reforestation using Thematic Mapper data, *Geocarto International*, 6 (1991) 31-37.

[60] P. Oliva, P. Martín, E. Chuvieco, Burned area mapping with MERIS post-fire image, *International journal of remote sensing*, 32 (2011) 4175-4201.

[61] J.M. Pereira, A.C. Sá, A.M. Sousa, J.M. Silva, T.N. Santos, J.M. Carreiras, Spectral characterisation and discrimination of burnt areas, *Remote sensing of large wildfires: In the European Mediterranean Basin*, (1999) 123-138.

[62] E. Roteta, A. Bastarrika, A. Ibisate, E. Chuvieco, A preliminary global automatic burned-area algorithm at medium resolution in Google Earth Engine, *Remote Sensing*, 13 (2021) 4298.

[63] C3C, Copernicus, <https://cds.climate.copernicus.eu/cdsapp#!/dataset/satellite-fire-burned-area>, (Access date : 28 May 2024).

[64] J. Lizundia-Loiola, M. Franquesa, M. Boettcher, G. Kirches, M.L. Pettinari, E. Chuvieco, Implementation of the burned area component of the Copernicus climate change service: from MODIS to OLCI data, *Remote Sensing*, 13 (2021) 4295.

[65] M.T.A.B.A.M.L.G.m.S. Grid, MODIS/Terra+Aqua Burned Area Monthly L3 Global 500 m SIN Grid, 2024.

[66] H. TONBUL, Google Earth Engine ile Türkiye'de Yanmış Alanların MODIS ve FireCCI51 Küresel Yanmış Alan Uydu Gözlem Verileriyle Karşılaştırmalı Değerlendirilmesi, *Turkish Journal of Remote Sensing and GIS*, 5 69-82.

[67] G. Petropoulos, W. Knorr, M. Scholze, L. Boschetti, G. Karantounias, Combining ASTER multispectral imagery analysis and support vector machines for rapid and cost-effective post-fire assessment: a case study from the Greek wildland fires of 2007, *Natural hazards and earth system sciences*, 10 (2010) 305-317.

- [68] D. Kalivas, G. Petropoulos, I. Athanasiou, V. Kollias, An intercomparison of burnt area estimates derived from key operational products: the Greek wildland fires of 2005–2007, *Nonlinear Processes in Geophysics*, 20 (2013) 397-409.
- [69] GEE, Google Earth Engine, <https://earthengine.google.com/> ,(Access date : 28 May 2024)
- [70] H. Tamiminia, B. Salehi, M. Mahdianpari, L. Quackenbush, S. Adeli, B. Brisco, Google Earth Engine for geo-big data applications: A meta-analysis and systematic review, *ISPRS journal of photogrammetry and remote sensing*, 164 (2020) 152-170.
- [71] L. Kumar, O. Mutanga, Google Earth Engine applications since inception: Usage, trends, and potential, *Remote sensing*, 10 (2018) 1509.
- [72] S.T. Seydi, M. Akhoondzadeh, M. Amani, S. Mahdavi, Wildfire damage assessment over Australia using sentinel-2 imagery and MODIS land cover product within the google earth engine cloud platform, *Remote Sensing*, 13 (2021) 220.
- [73] E. Roteta, A. Bastarrika, M. Franquesa, E. Chuvieco, Landsat and sentinel-2 based burned area mapping tools in google earth engine, *Remote Sensing*, 13 (2021) 816.
- [74] P. Liu, Y.X. Liu, X.X. Guo, W.J. Zhao, H.S. Wu, W.X. Xu, Burned area detection and mapping using time series Sentinel-2 multispectral images, *Remote Sens Environ*, 296 (2023).
- [75] S. Trigg, S. Flasse, An evaluation of different bi-spectral spaces for discriminating burned shrub-savannah, *International Journal of Remote Sensing*, 22 (2001) 2641-2647.
- [76] E. Chuvieco, M.P. Martin, A. Palacios, Assessment of different spectral indices in the red-near-infrared spectral domain for burned land discrimination, *International Journal of Remote Sensing*, 23 (2002) 5103-5110.
- [77] C.J. Tucker, Red and photographic infrared linear combinations for monitoring vegetation, *Remote Sens Environ*, 8 (1979) 127-150.
- [78] E. Çolak, F. Sunar, Cycle-Gan Based Feature Translation for Optical-Sar Data in Burned Area Mapping, *The International Archives of the Photogrammetry, Remote Sensing and Spatial Information Sciences*, 48 (2023) 491-496.

- [79] B. Wu, H. Zheng, Z. Xu, Z. Wu, Y. Zhao, Forest burned area detection using a novel spectral index based on multi-objective optimization, *Forests*, 13 (2022).
- [80] T. Kavzoglu, M. Yildiz, H. Tonbul, Evaluating performances of spectral indices for burned area mapping using object-based image analysis, 12th International symposium on spatial accuracy assessment in natural resources and environmental sciences, 2016, pp. 5-8.
- [81] U.C. Benz, P. Hofmann, G. Willhauck, I. Lingenfelder, M. Heynen, Multi-resolution, object-oriented fuzzy analysis of remote sensing data for GIS-ready information, *ISPRS Journal of photogrammetry and remote sensing*, 58 (2004) 239-258.
- [82] M.D. Hossain, D. Chen, Segmentation for Object-Based Image Analysis (OBIA): A review of algorithms and challenges from remote sensing perspective, *ISPRS Journal of Photogrammetry and Remote Sensing*, 150 (2019) 115-134.
- [83] H. Tonbul, T. Kavzoğlu, Nesne-Tabanlı Sınıflandırmada Segmentasyon (Bölütleme) Kalitesinin Sınıflandırma Doğruluğu Üzerine Etkisinin İncelenmesi, *Afyon Kocatepe Üniversitesi Fen ve Mühendislik Bilimleri Dergisi*, (2017) 118-125.
- [84] R. Achanta, S. Susstrunk, Superpixels and polygons using simple non-iterative clustering, *Proceedings of the IEEE conference on computer vision and pattern recognition*, 2017, pp. 4651-4660.
- [85] H. Shafizadeh-Moghadam, M. Khazaei, S.K. Alavipanah, Q. Weng, Google Earth Engine for large-scale land use and land cover mapping: An object-based classification approach using spectral, textural and topographical factors, *GIScience & Remote Sensing*, 58 (2021) 914-928.
- [86] A. Tassi, M. Vizzari, Object-oriented lulc classification in google earth engine combining snic, glcm, and machine learning algorithms, *Remote Sensing*, 12 (2020) 3776.
- [87] M. Mahdianpari, B. Salehi, F. Mohammadimanesh, S. Homayouni, E. Gill, The first wetland inventory map of newfoundland at a spatial resolution of 10 m using sentinel-1 and sentinel-2 data on the google earth engine cloud computing platform, *Remote Sensing*, 11 (2018) 43.

- [88] Medium, Medium Object Based Image Analysis on Google Earth Engine, <https://joaootavionf007.medium.com/object-based-image-analysis-on-google-earth-engine-1b80e9cb7312>, (Access date : 28 May **2024**)
- [89] L. Breiman, Random forests, *Machine learning*, 45 (**2001**) 5-32.
- [90] J. Stefanski, B. Mack, B. Waske, Optimization of object-based image analysis with random forests for land cover mapping, *IEEE Journal of Selected Topics in Applied Earth Observations and Remote Sensing*, 6 (**2013**) 2492-2504.
- [91] S. Amini, S. Homayouni, A. Safari, A.A. Darvishsefat, Object-based classification of hyperspectral data using Random Forest algorithm, *Geo-spatial information science*, 21 (**2018**) 127-138.
- [92] D.R. Cutler, T.C. Edwards Jr, K.H. Beard, A. Cutler, K.T. Hess, J. Gibson, J.J. Lawler, Random forests for classification in ecology, *Ecology*, 88 (**2007**) 2783-2792.
- [93] S. Praticò, F. Solano, S. Di Fazio, G. Modica, Machine learning classification of mediterranean forest habitats in google earth engine based on seasonal sentinel-2 time-series and input image composition optimisation, *Remote Sensing*, 13 (**2021**) 586.
- [94] M. Rejaur Rahman, S. Saha, Multi-resolution segmentation for object-based classification and accuracy assessment of land use/land cover classification using remotely sensed data, *Journal of the Indian Society of Remote Sensing*, 36 (**2008**) 189-201.
- [95] J.R. Jensen, *Introductory digital image processing: a remote sensing perspective*, (**1996**).
- [96] J. Cohen, A coefficient of agreement for nominal scales, *Educational and psychological measurement*, 20 (**1960**) 37-46.
- [97] L. Ma, L. Cheng, M. Li, Y. Liu, X. Ma, Training set size, scale, and features in Geographic Object-Based Image Analysis of very high resolution unmanned aerial vehicle imagery, *ISPRS Journal of Photogrammetry and Remote Sensing*, 102 (**2015**) 14-27.
- [98] L.a. Qu, Z. Chen, M. Li, J. Zhi, H. Wang, Accuracy improvements to pixel-based and object-based lulc classification with auxiliary datasets from Google Earth engine, *Remote Sensing*, 13 (**2021**) 453.

[99] G. Yang, W. Yu, X. Yao, H. Zheng, Q. Cao, Y. Zhu, W. Cao, T. Cheng, AGTOC: A novel approach to winter wheat mapping by automatic generation of training samples and one-class classification on Google Earth Engine, *International Journal of Applied Earth Observation and Geoinformation*, 102 (2021) 102446.